Supporting Information

From helix to superhelix: hierarchical assembly of homochiral van der Waals 1D coordination polymers

Guo-Guo Weng,[a] Ben-Kun Hong,[b] Song-Song Bao,[a] Yujie Wen,[c] Lan-Qing Wu,[a] Xin-Da Huang,[a] Jia-Ge Jia,[a] Ge-Hua Wen,[a] Shu-Hua Li,[b] Luming Peng,[c] Li-Min Zheng*[a]

[a]State Key Laboratory of Coordination Chemistry, School of Chemistry and Chemical Engineering, Collaborative Innovation Center of Advanced Microstructures, Nanjing University, Nanjing 210023, P. R. China. Emial: lmzheng@nju.edu.cn

[b]Institute of Theoretical and Computational Chemistry, School of Chemistry and Chemical Engineering, Nanjing University, Nanjing 210023, People's Republic of China.

[c] Key Laboratory of Mesoscopic Chemistry of MOE and Collaborative Innovation Center of Chemistry for Life Sciences, School of Chemistry and Chemical Engineering, Nanjing University, Nanjing 210023, People's Republic of China

Table S1. Crystallographic data for ***S*-2C** and ***R*-2C**.

Compound	***S*-2C**	***R*-2C**
Formula	$C_{29}H_{65}N_3O_{13}P_3Tb$	$C_{29}H_{65}N_3O_{13}P_3Tb$
M	915.67	915.67
Temperature (K)	193	193
Crystal system	hexagonal	hexagonal
Space group	$P6_1$	$P6_5$
a (Å)	17.0310(6)	17.0143(5)
b (Å)	17.0310(6)	17.0143(5)
c (Å)	23.5742(12)	23.5290(10)
V (Å^3)	5921.7(5)	5898.8(4)
Z	6	6
*D*c (g cm^{-3})	1.541	1.547
μ (mm^{-1})	10.389	1.982
F(000)	2844	2844
R_{int}	0.0804	0.0512
GOF	1.035	1.039
R_1, wR_2 [I>2σ(I)]	0.0368, 0.0889	0.0255, 0.0574
R_1, wR_2 (all data)	0.0395, 0.0907	0.0295, 0.0597
Flack parameter	-0.009(3)	-0.010(5)
CCDC	2034187	2034186

$^aR_1 = \sum||F_o|-|F_c||/ \sum|F_o|$. $wR_2 = [\sum w(F_o^2-F_c^2)^2/ \sum w(F_o^2)^2]^{1/2}$

Table S2. Selected bond lengths (Å) and bond angles (°) for ***S*-2C** at 193 K.

Tb1-O7	2.280(4)	P1-O3	1.499(4)
Tb1-O5A	2.312(4)	P1-O2	1.523(4)
Tb1-O8A	2.329(4)	P1-O1	1.535(4)
Tb1-O1B	2.352(4)	P2-O6	1.494(5)
Tb1-O2	2.417(4)	P2-O4	1.525(4)
Tb1-O5	2.468(4)	P2-O5	1.530(5)
Tb1-O4	2.471(4)	P3-O9	1.508(5)
Tb1-O1	2.518(4)	P3-O7	1.514(5)
		P3-O8	1.523(4)
O7-Tb1-O5A	80.65(15)	O2-Tb1-O5	85.83(13)
O7-Tb1-O8A	86.04(17)	O7-Tb1-O4	93.47(16)
O5A-Tb1-O8A	80.95(15)	O5A-Tb1-O4	71.83(14)
O7-Tb1-O1B	83.94(15)	O8A-Tb1-O4	152.46(14)
O5A-Tb1-O1B	156.91(13)	O1B-Tb1-O4	126.47(14)
O8A-Tb1-O1B	80.92(15)	O2-Tb1-O4	87.68(13)
O7-Tb1-O2	155.20(14)	O5-Tb1-O4	58.52(14)
O5A-Tb1-O2	122.90(14)	O7-Tb1-O1	145.25(14)
O8A-Tb1-O2	104.10(15)	O5A-Tb1-O1	69.39(13)
O1B-Tb1-O2	75.60(14)	O8A-Tb1-O1	72.54(14)
O7-Tb1-O5	73.85(15)	O1B-Tb1-O1	117.97(14)
O5A-Tb1-O5	121.44(15)	O2-Tb1-O1	59.13(13)
O8A-Tb1-O5	145.63(15)	O5-Tb1-O1	137.11(12)
O1B-Tb1-O5	69.66(14)	O4-Tb1-O1	93.52(13)

Symmetry codes: A: y, -x+y, z-1/6; B: x-y, x, z+1/6.

Table S3. Hydrogen bonds in ***S*-2C**.

D-H...A	d(D-H)	d(H...A)	d(D...A)	<DHA (°)
O10-H10C...O9	0.88	1.67	2.517(7)	160.3
O1W-H1WA...O6	0.95	1.89	2.771(10)	152.5
O2W-H2WA...O3	0.95	1.98	2.790(7)	141.3
O2W-H2WB...O2A	0.95	2.18	2.868(6)	128.7
N1-H1C...O3B	0.91	1.76	2.661(7)	171.1
N1-H1D...O8A	0.91	2.29	3.163(7)	159.7
N2-H2A...O4B	0.91	1.93	2.738(7)	147.6
N2-H2B...O2W	0.91	2.03	2.919(7)	165.7
N3-H3D...O9B	0.91	2.41	3.131(7)	136.5
N3-H3E...O6	0.91	1.97	2.853(7)	162.2

Symmetry codes: A: y, -x+y, z-1/6; B: x-y, x, z+1/6.

Table S4. Selected bond lengths (Å) and bond angles (°) for ***R*-2C** at 193 K.

Tb1-O7	2.271(4)	P1-O3	1.505(4)
Tb1-O5A	2.313(4)	P1-O2	1.522(4)
Tb1-O8A	2.328(4)	P1-O1	1.528(4)
Tb1-O1B	2.347(4)	P2-O6	1.497(4)
Tb1-O2	2.413(3)	P2-O5	1.525(4)
Tb1-O4	2.465(3)	P2-O4	1.527(4)
Tb1-O5	2.466(4)	P3-O9	1.512(4)
Tb1-O1	2.518(4)	P3-O8	1.519(4)
		P3-O7	1.520(4)
O7-Tb1-O5A	80.43(13)	O2-Tb1-O4	87.38(11)
O7-Tb1-O8A	86.00(13)	O7-Tb1-O5	73.90(13)
O5A-Tb1-O8A	81.07(13)	O5A-Tb1-O5	121.17(13)
O7-Tb1-O1B	84.05(13)	O8A-Tb1-O5	145.70(13)
O5A-Tb1-O1B	156.80(10)	O1B-Tb1-O5	69.95(12)
O8A-Tb1-O1B	80.73(13)	O2-Tb1-O5	85.89(11)
O7-Tb1-O2	155.25(13)	O4-Tb1-O5	58.53(12)
O5A-Tb1-O2	123.07(13)	O7-Tb1-O1	145.20(13)
O8A-Tb1-O2	104.04(12)	O5A-Tb1-O1	69.56(12)
O1B-Tb1-O2	75.54(11)	O8A-Tb1-O1	72.61(12)
O7-Tb1-O4	93.86(13)	O1B-Tb1-O1	117.87(12)
O5A-Tb1-O4	71.84(11)	O2-Tb1-O1	59.13(12)
O8A-Tb1-O4	152.51(12)	O4-Tb1-O1	93.16(11)
O1B-Tb1-O4	126.65(13)	O5-Tb1-O1	137.04(10)

Symmetry codes: A: y, -x+y+1, z+1/6; B: x-y+1, x, z-1/6.

Table S5. Hydrogen bonds in ***R*-2C**.

D-H...A	d(D-H)	d(H...A)	d(D...A)	<DHA (°)
O10-H10C...O9	0.88	1.64	2.511(6)	167.3
O1W-H1WA...O6	0.95	1.86	2.775(9)	160.3
O2W-H2WA...O3	0.95	2.31	2.786(5)	110.4
O2W-H2WB...O2A	0.96	1.96	2.869(5)	156.7
N1-H1D...O3B	0.91	1.75	2.657(6)	171.8
N1-H1C...O8A	0.91	2.28	3.147(5)	158.9
N2-H2A...O2W	0.91	2.02	2.910(6)	165.0
N2-H2B...O4B	0.91	1.92	2.732(6)	148.4
N3-H3D...O6	0.91	1.96	2.838(6)	161.6
N3-H3E...O9B	0.91	2.40	3.120(6)	136.1

Symmetry transformations used to generate equivalent atoms:
A: y, -x+y+1, z+1/6; B: x-y+1, x, z-1/6.

Table S6 Structural comparison of Tb(R-cyampH)$_3$·HOAc·2H_2O, Tb(R-pempH)$_3$·H_2O and [Tb$_3$(R-pempH$_2$)$_2$(R-pempH)$_7$](NO_3)$_2$·2H_2O.

Compounds	**Tb(*R*-cyampH)$_3$·HOAc·2H_2O** (this work)	**Tb(*R*-pempH)$_3$·H_2O** (Nat. Commun. 2017, 8, 2131)	**[Tb$_3$(*R*-pempH$_2$)$_2$(*R*-pempH)$_7$] (NO_3)$_2$·2H_2O** (Nat. Commun. 2017, 8, 2131)
Different ligands	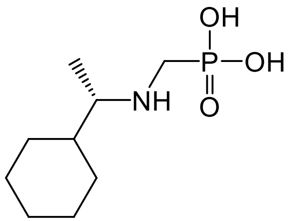 Terminal organic part: cyclohexyl	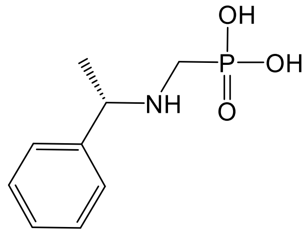 Terminal organic part: phenyl	
Similar coordination geometry	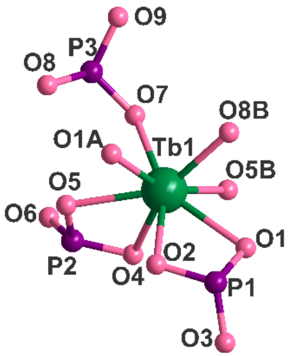 {Tb1O_8} Tb-O: 2.279(4)–2.518(4) Å O-Tb-O: 58.5(1)–156.9(1)°	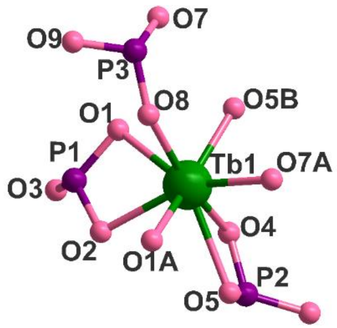 {Tb1O_8} Tb-O: 2.28(2)–2.632(16) Å O-Tb-O: 58.1(5)–162.2(5)°	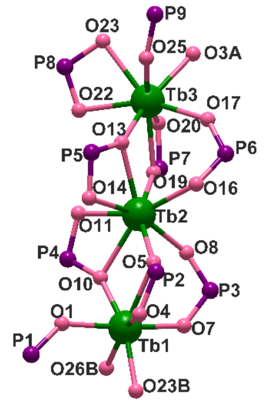 {Tb1O_7}, {Tb2O_8} and {Tb3O_8} Tb-O: 2.253(7)–2.563(7) Å O-Tb-O: 57.8(1)–159.1(1)°

<table>
<tr>
<td>Helical chains</td>
<td>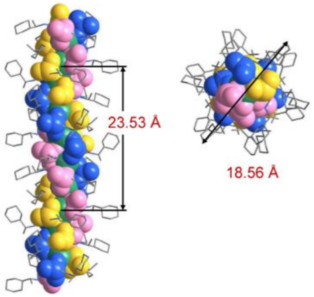
</td>
<td>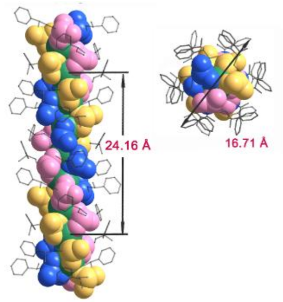
</td>
<td>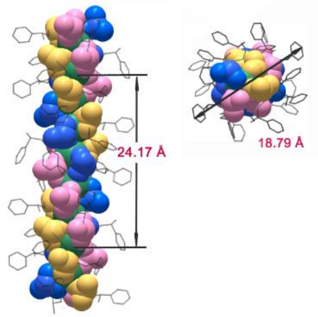
</td>
</tr>
<tr>
<td>Intrachain H-bonds involving -NH2- groups</td>
<td>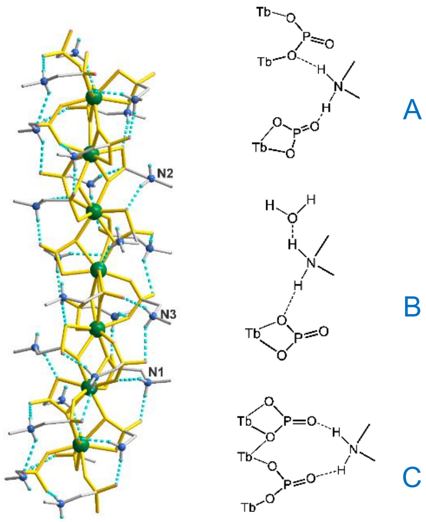

three modes: A, B and C</td>
<td>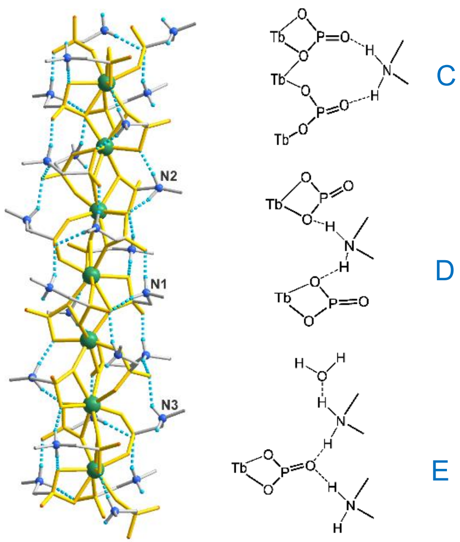

three modes: C, D and E</td>
<td>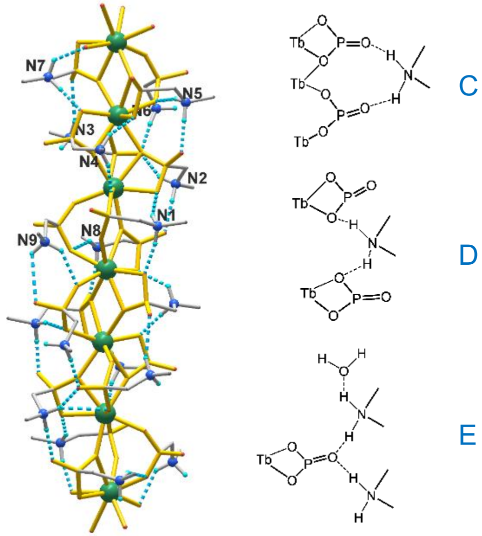
</td>
</tr>
</table>

			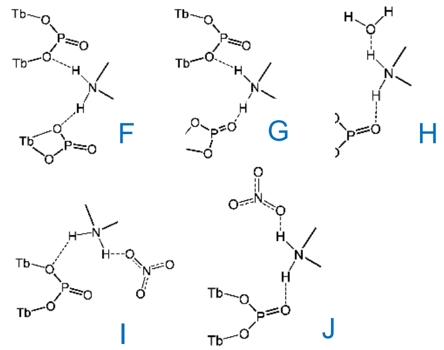 Eight modes: C, D, E, F, G, H, I and J
H-bonds involving -lattice molecules or anions	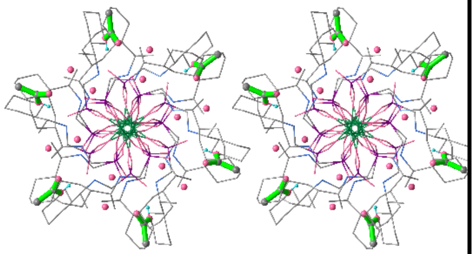 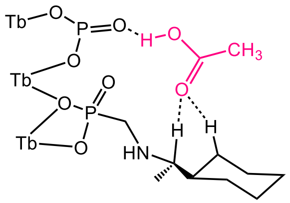 H-bonds between one chain and HOAc molecules	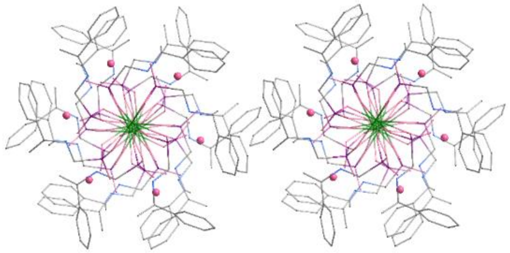	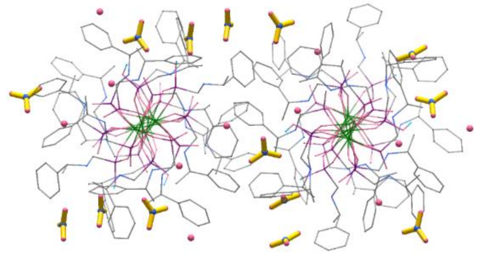 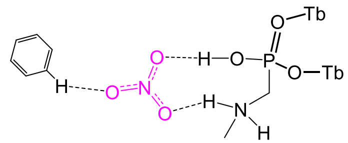

			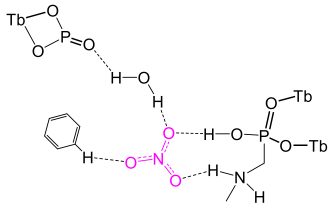 H-bonds between two chains and NO_3^- molecules
Interchain interactions	only vdW interactions short C…C distances between two chains 3.78(1), 3.80(2), 3.77(1), 3.76(2) Å	vdW and C-H…π interactions short C…C distances between two chains 3.54(1), 3.58(1), 3.80(1) Å C…Cgs distances (C-H…π) 3.69(1) Å (methyl C…phenyl ring)	only vdW interactions short C…C distances between two chains 3.62(1), 3.77(1) Å
Interchain distance	17.031 Å	15.824 Å	15.342 Å, 16.987 Å

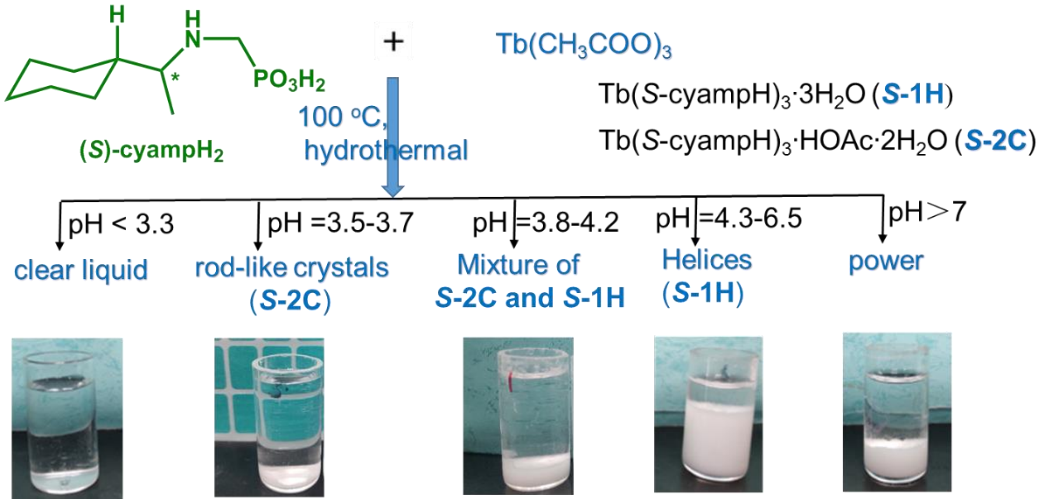

Figure S1. Summary of pH regulation results of *S*-cyampH_2 / Tb$(OAc)_3$.

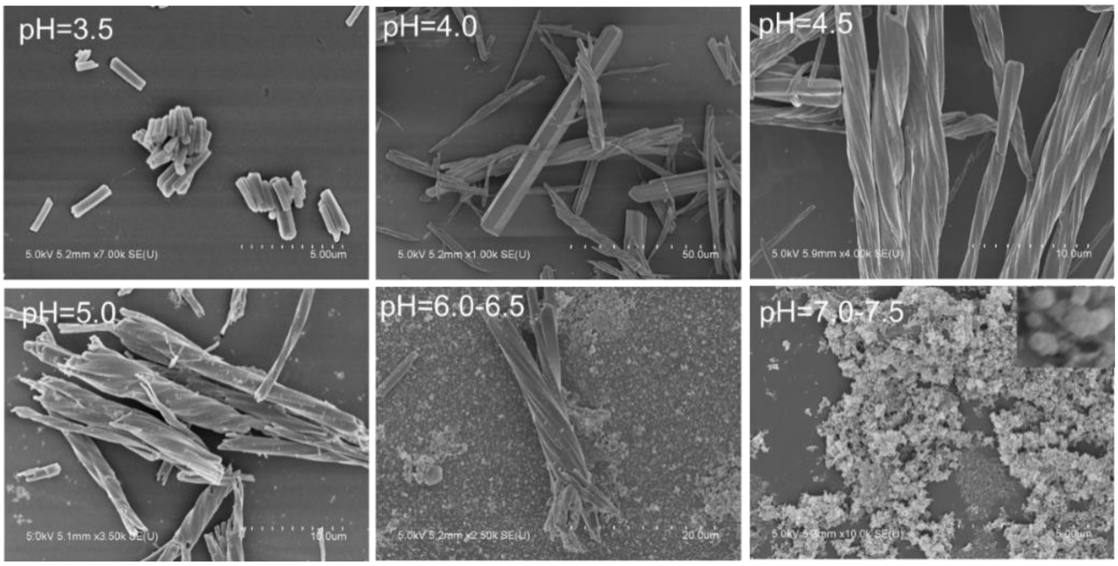

Figure S2. SEM images of the reaction products of Tb$(OAc)_3$ and *S*-cyampH_2 at 100 °C and 24 h for different pH values.

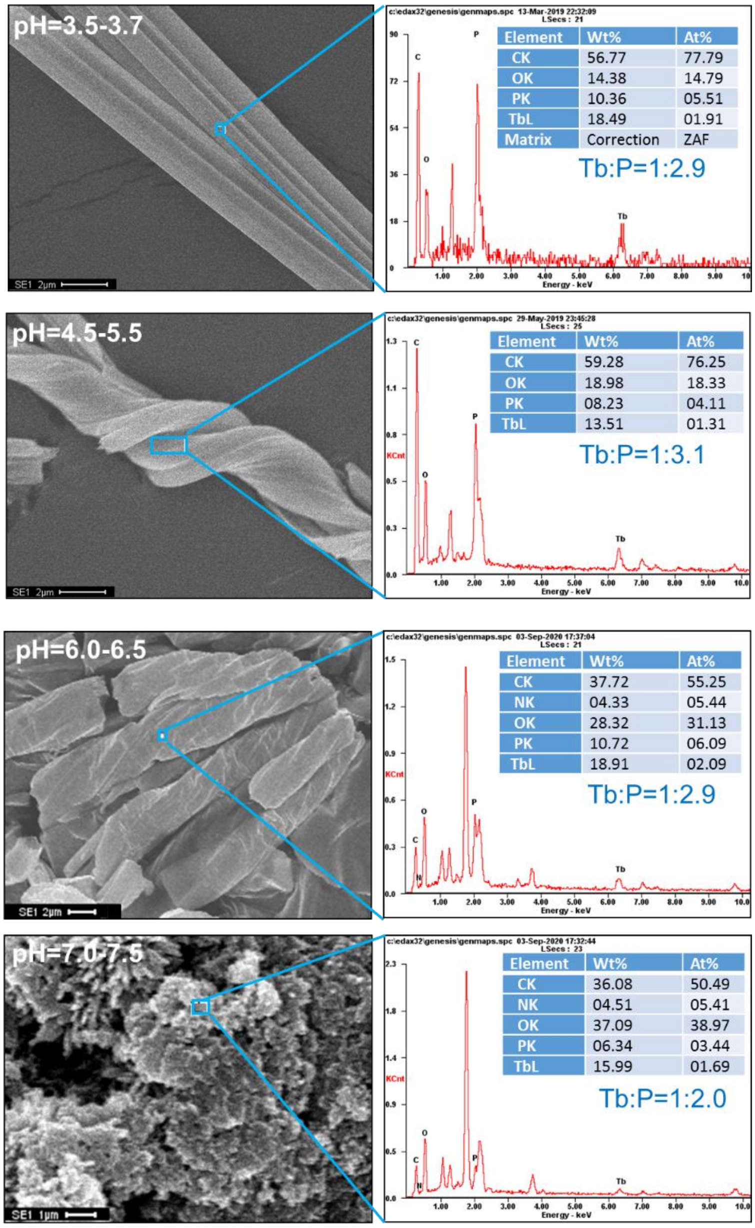

Figure S3. EDX images of the reaction products of $Tb(OAc)_3$ and *S*-cyampH_2 at 100 °C and 24 h for different pH values.

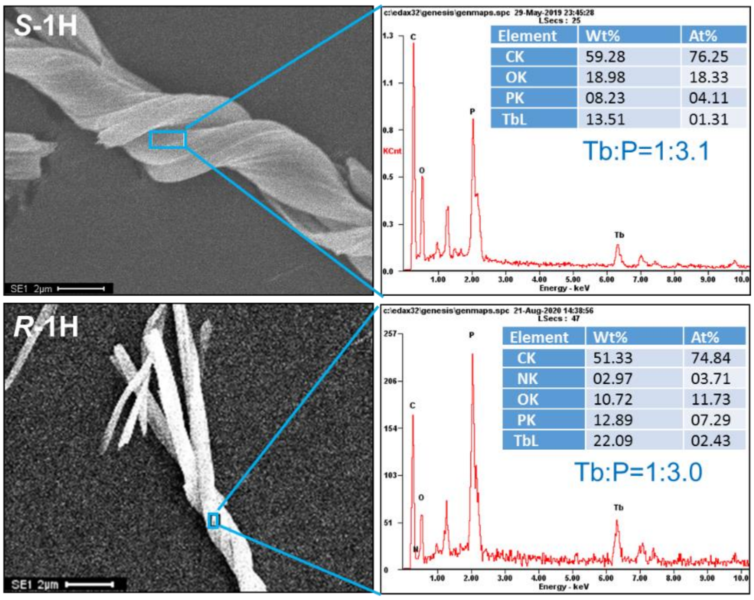

Figure S4. EDX spectra of ***S*-1H** and ***R*-1H** helices.

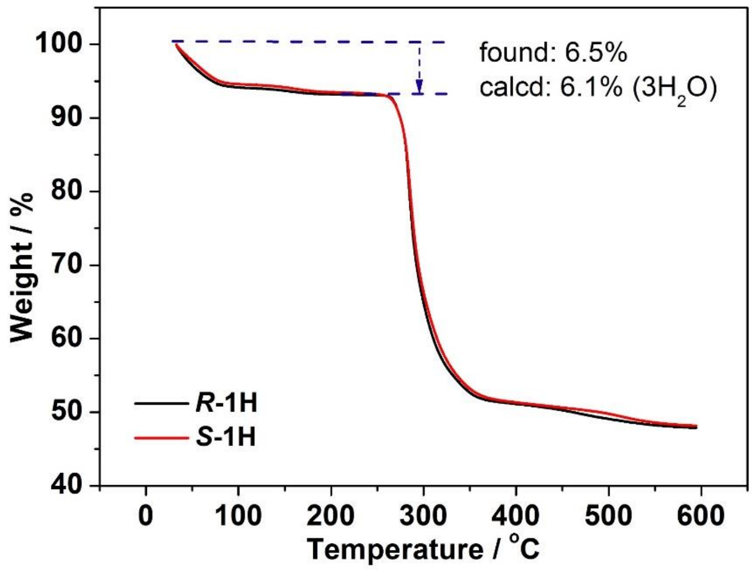

Figure S5. TG analyses of ***S*-1H** and ***R*-1H**.

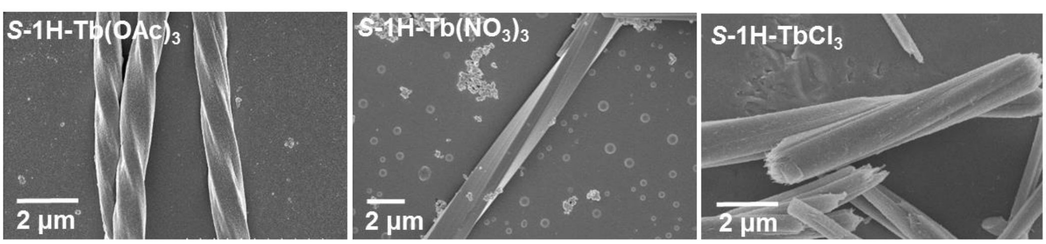

Figure S6. SEM images of ***S*-1H** obtained under similar hydrothermal reaction conditions (pH = 4.5, 100 °C, 24 h) except using different terbium salt.

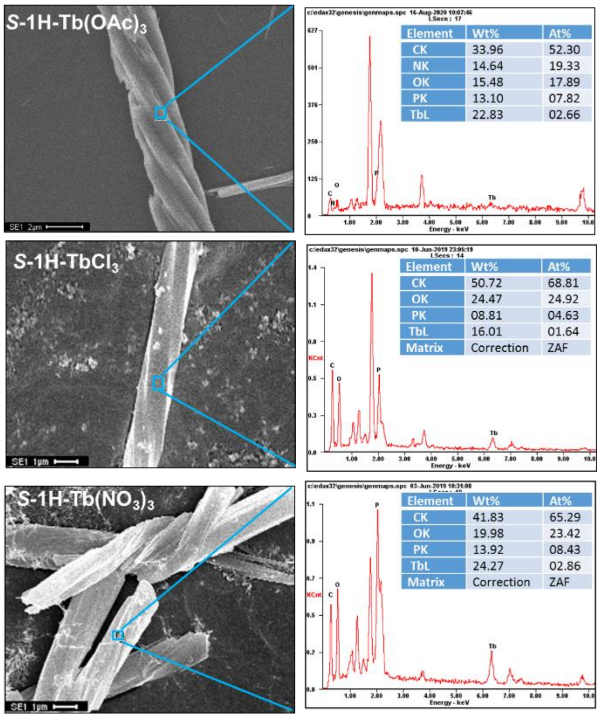

Figure S7. EDX spectra of ***S*-1H** obtained under similar hydrothermal reaction conditions (pH = 4.5, 100 °C, 24 h) except using different terbium salt.

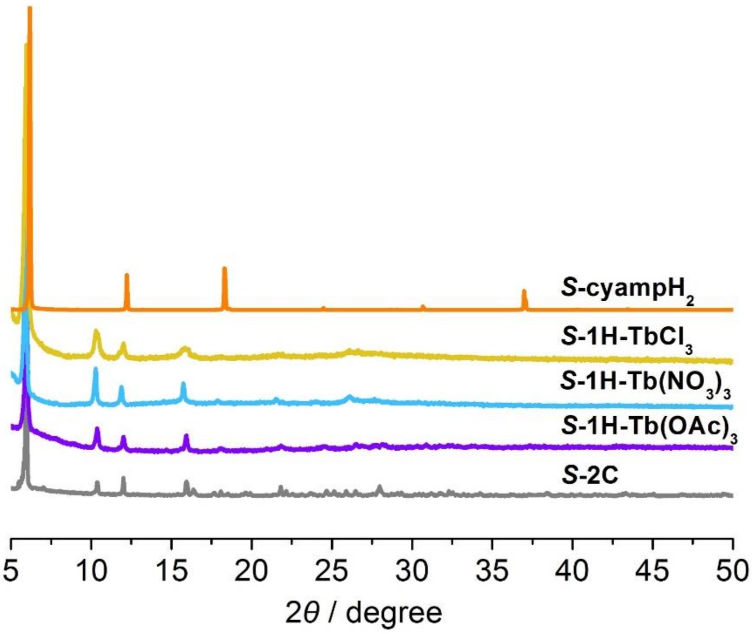

Figure S8. PXRD patterns of ***S*-1H** obtained under similar hydrothermal reaction conditions (pH = 4.5, 100 °C, 24 h) except using different terbium salt.

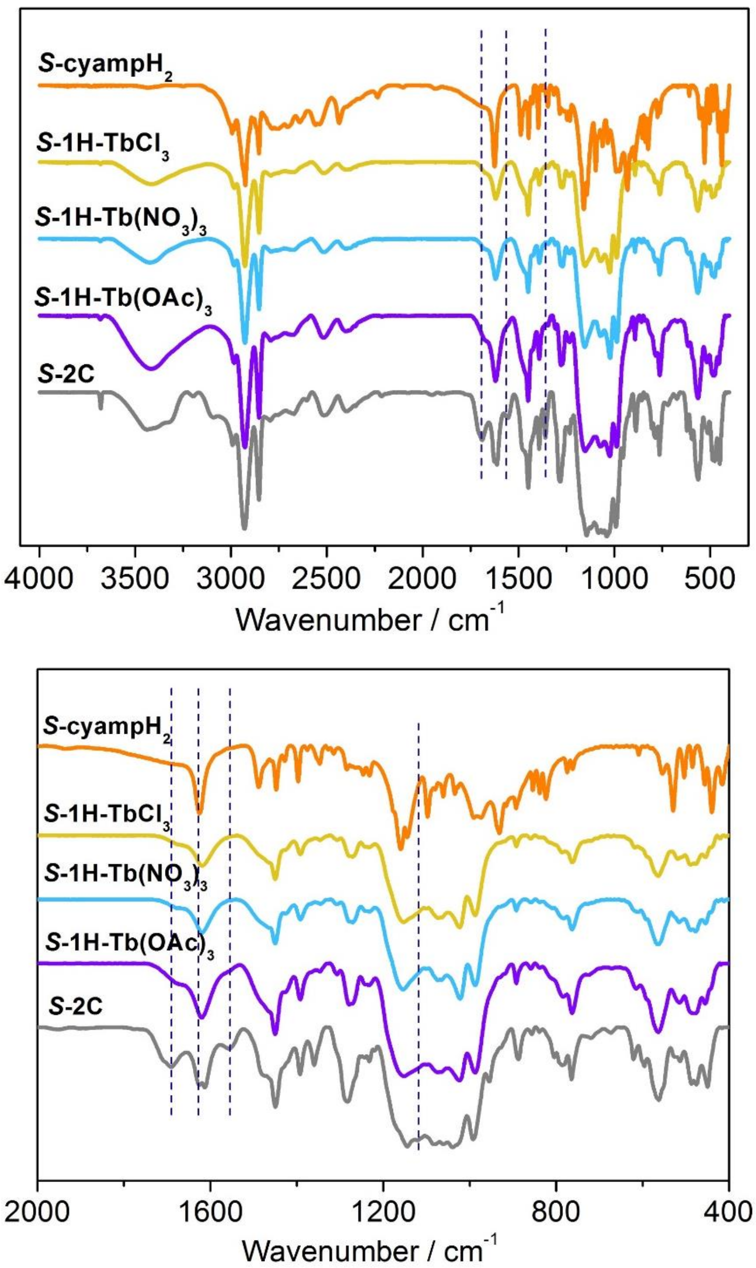

Figure S9. Infrared spectra (IR) of ***S*-1H** obtained under similar hydrothermal reaction conditions (pH = 4.5, 100 °C, 24 h) except using different terbium salt.

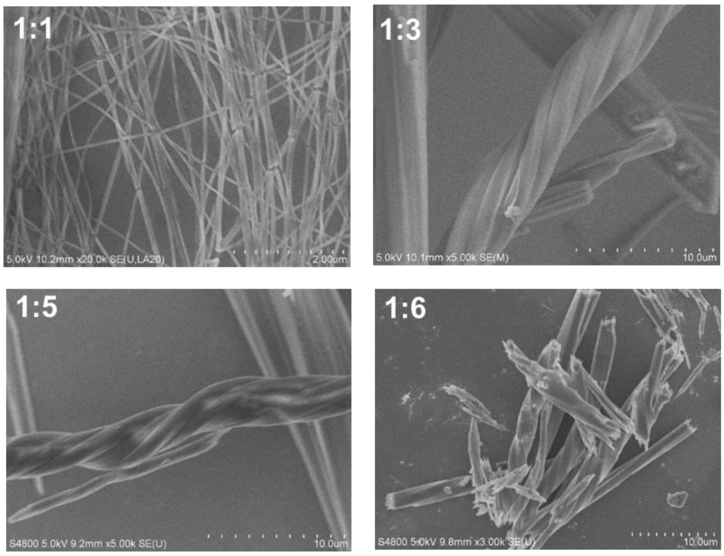

Figure S10. SEM images of products obtained under similar hydrothermal reaction conditions (pH = 4.5, 100 °C, 24 h) except using different Tb/P molar ratio.

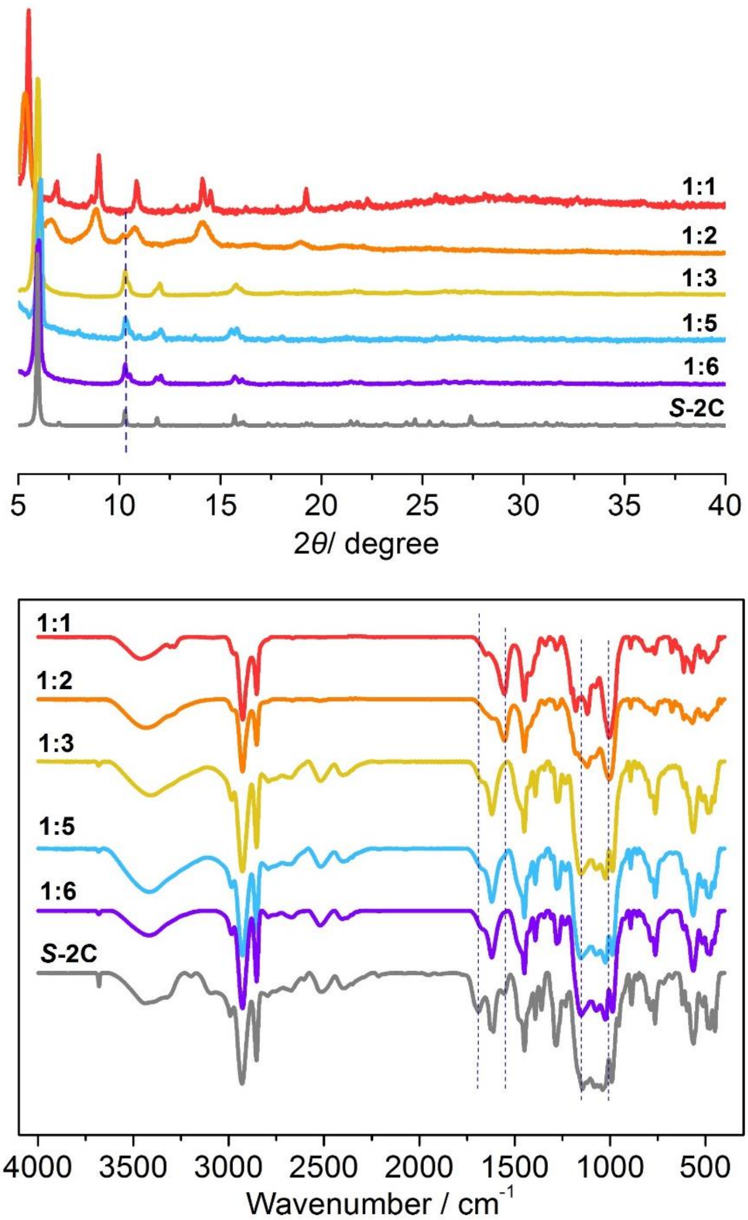

Figure S11. PXRD patterns (top) and infrared spectra (bottom) of products obtained under similar hydrothermal reaction conditions (pH = 4.5, 100 °C, 24 h) except using different Tb/P molar ratio.

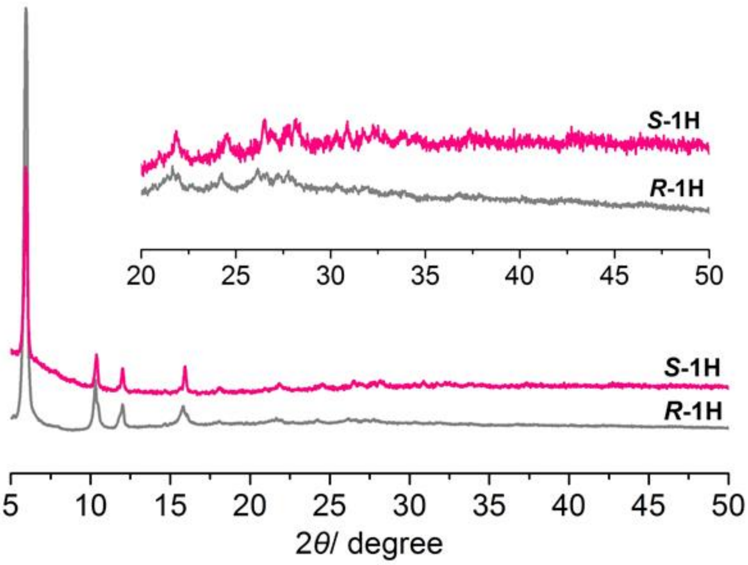

Figure S12. PXRD patterns of ***S*-1H** and ***R*-1H.**

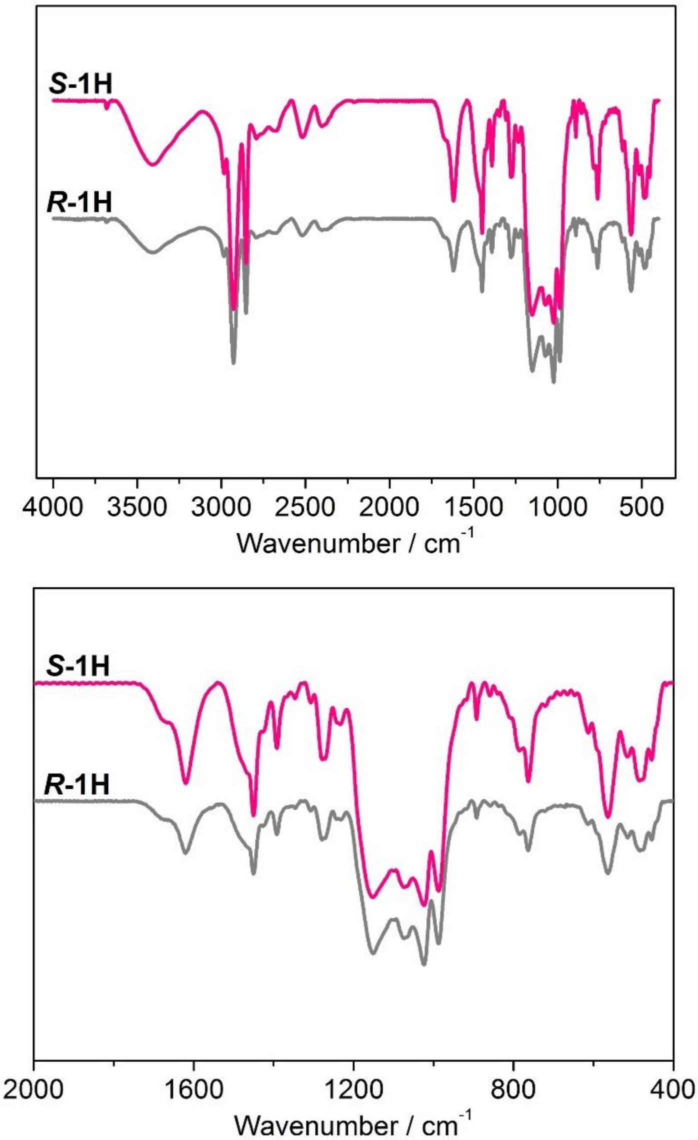

Figure S13. Infrared spectra of ***S*-1H** and ***R*-1H**.

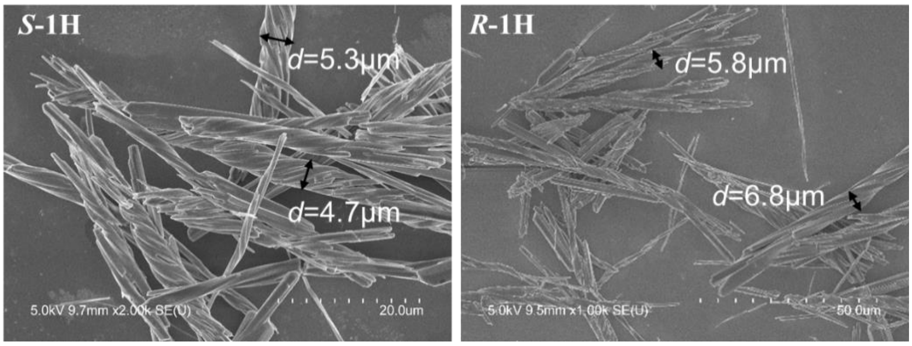

Figure S14. SEM images of ***S*-1H** and ***R*-1H.**

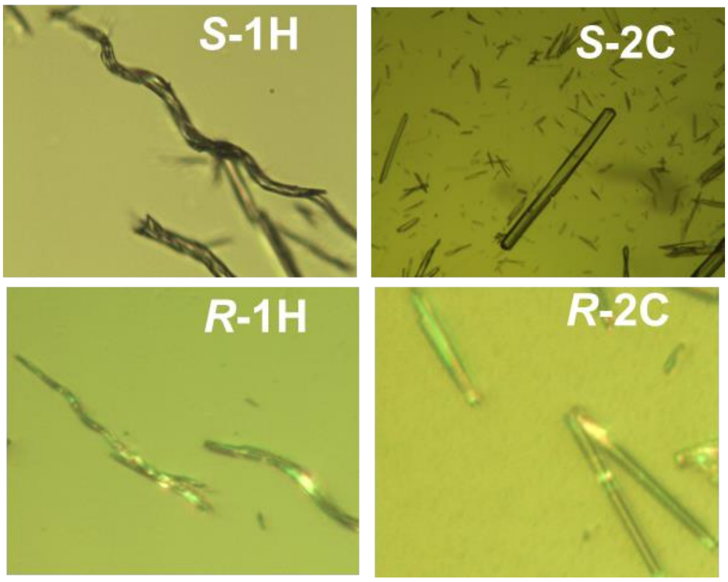

Figure S15. Optical photographs of ***S*-1H**, ***R*-1H**, ***S*-2C**, and ***R*-2C**.

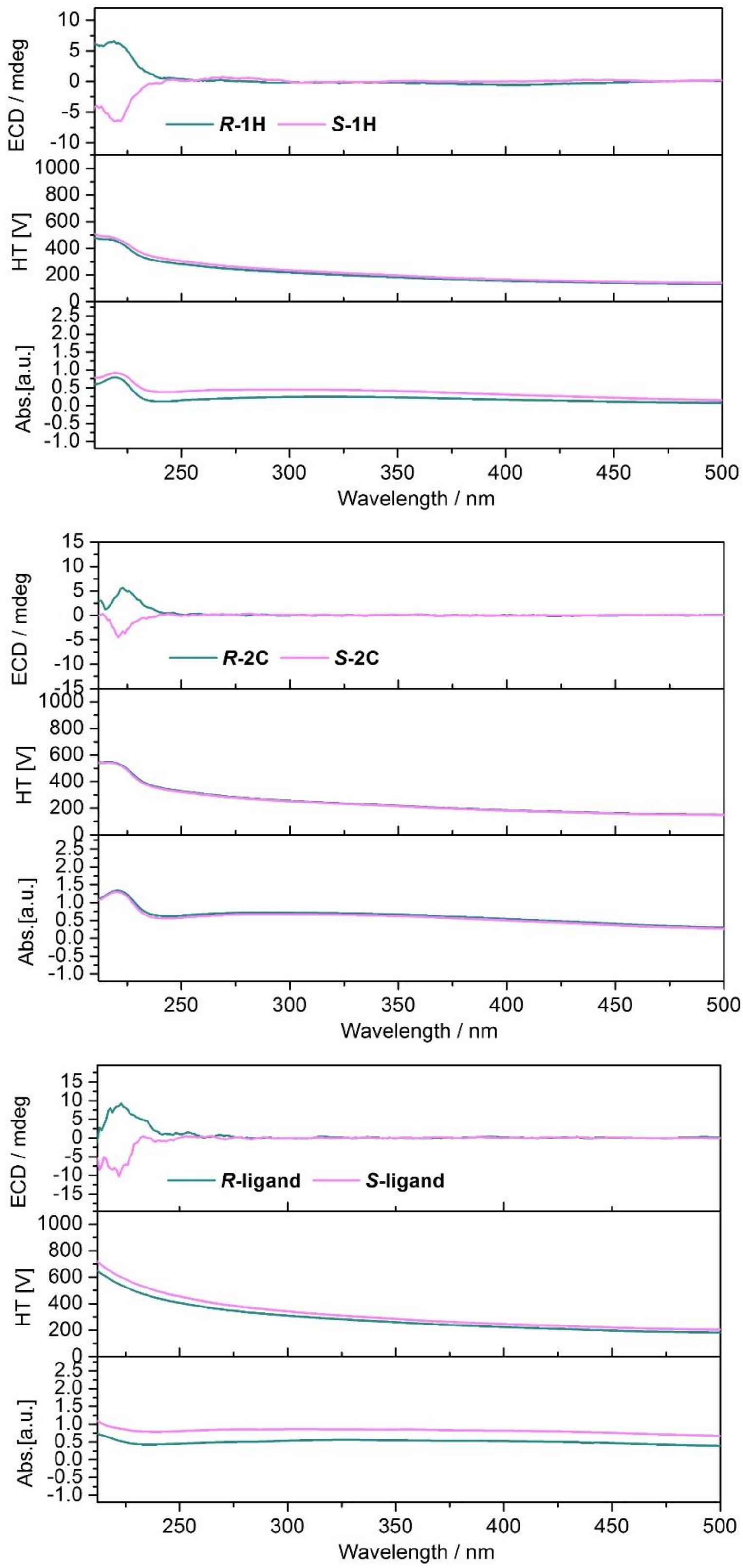

Figure S16. ECD spectra of *S*- and *R*-isomers of **1H** superhelices, **2C** crystals and cyampH_2 ligands.

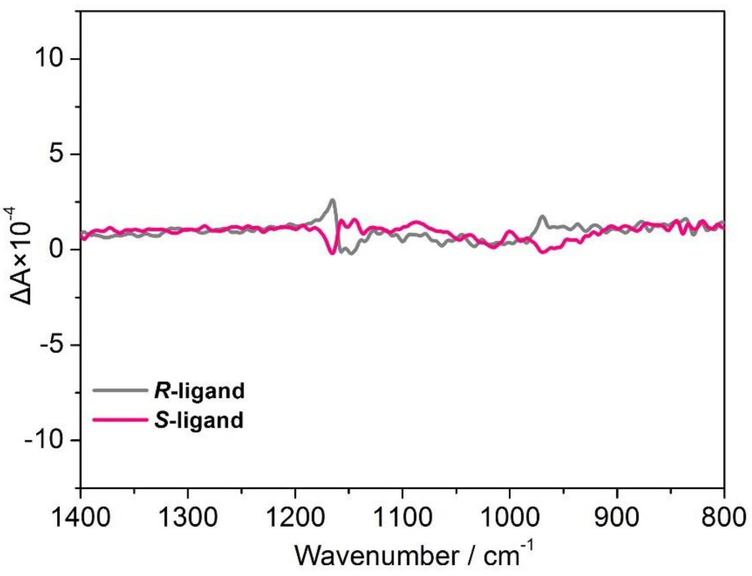

Figure S17. VCD spectra of *S*- and *R*-cyampH$_2$ ligands.

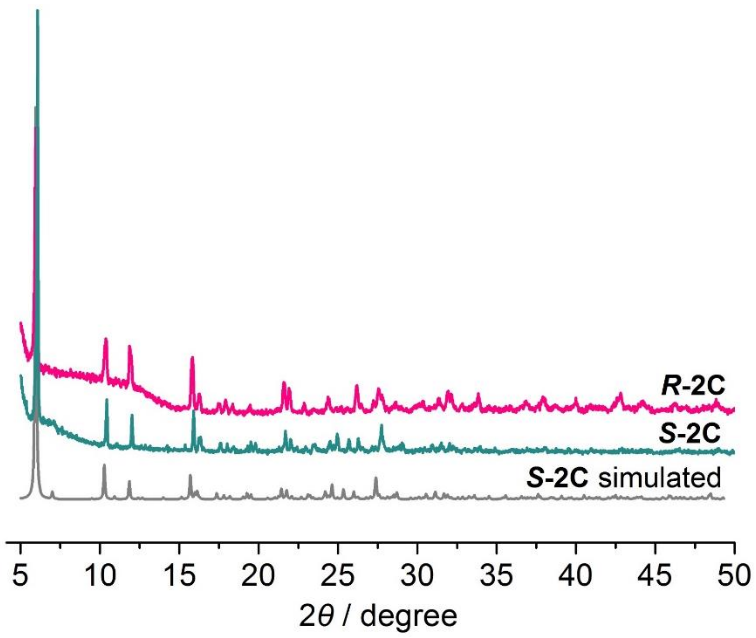

Figure S18. PXRD patterns of ***S*-2C** and ***R*-2C**

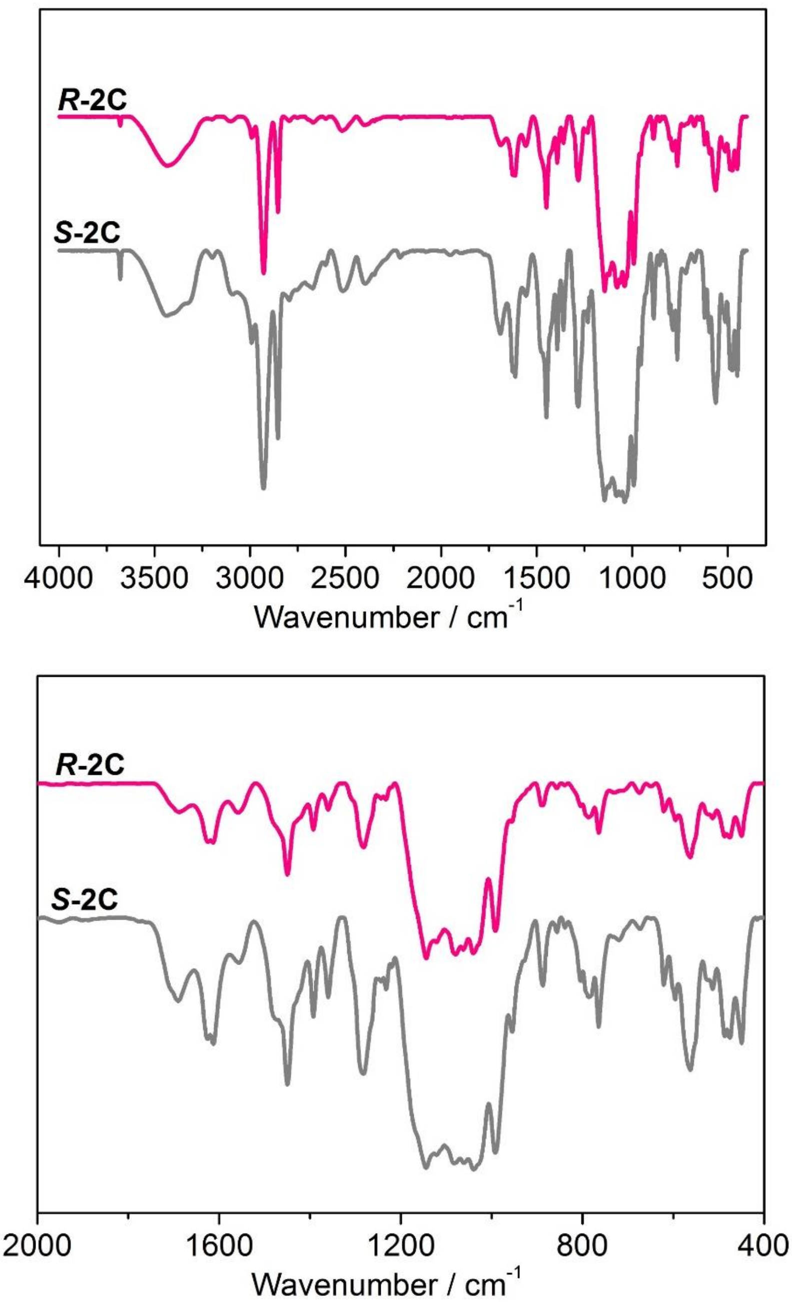

Figure S19. Infrared spectra of ***S*-2C** and ***R*-2C**.

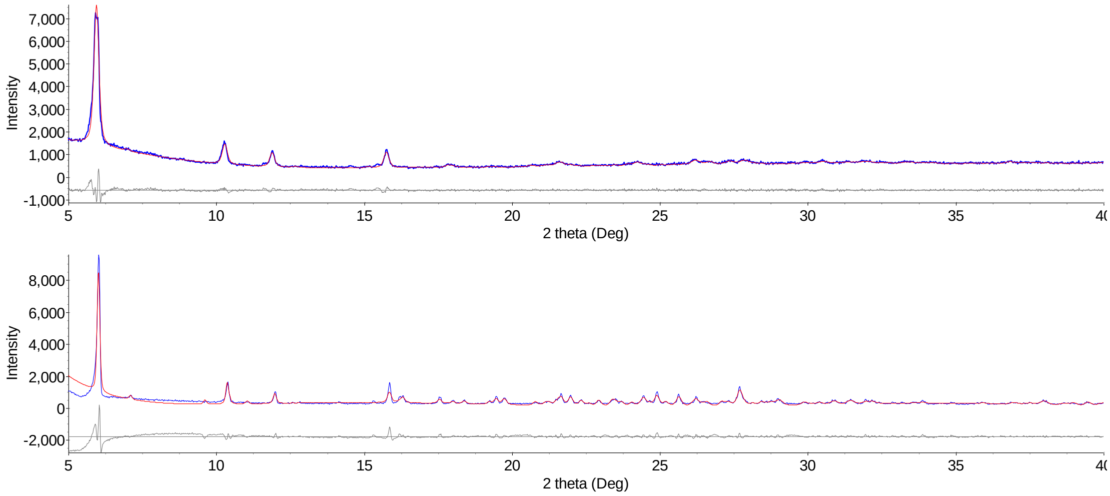

Figure S20. Pawley fit of powder samples of ***S*-1H** (top) and ***S*-2C** (bottom) using Topas 5.0 program

The diffraction peaks can be indexed by using TOPAS 5.0 program, giving a set of unit cell parameters with space group $P6_1$, a = 17.21 Å, c = 23.77 Å and V = 6094.30 Å^3 for ***S*-1H** (Figure S20, top). And the diffraction peaks of ***S*-2C** can also be simulated to get a set of unit cell parameters with space group, a = 17.13 Å, c = 23.67 Å and V = 6016.89 Å^3 for ***S*-2C** (Figure S20, bottom).

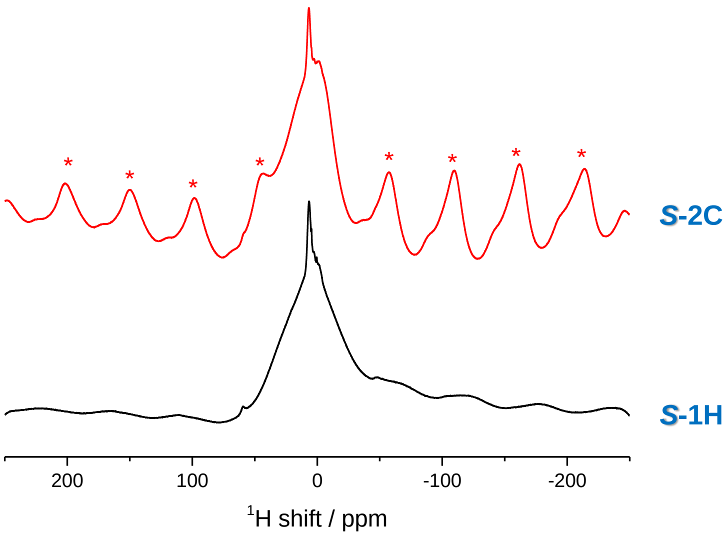

Figure S21. ^{1}H MAS NMR of ***S*-1H** and ***S*-2C**. Asterisks denote spinning sidebands.

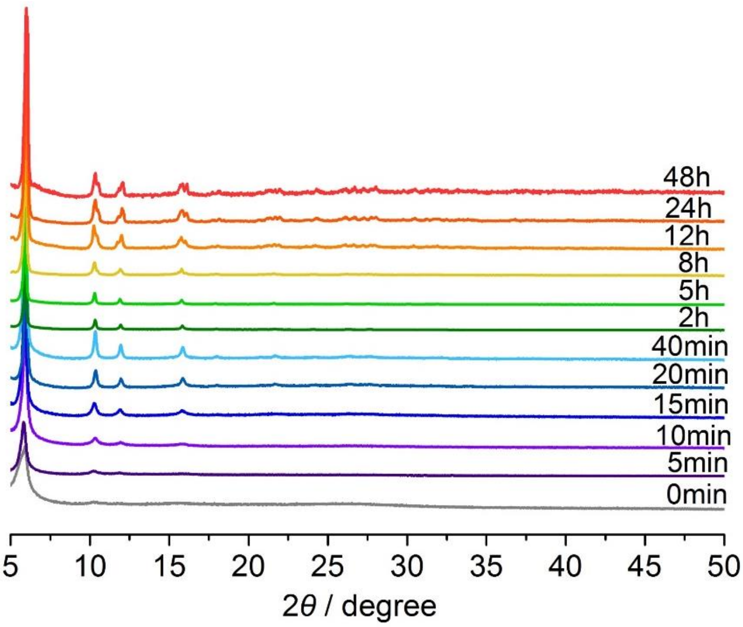

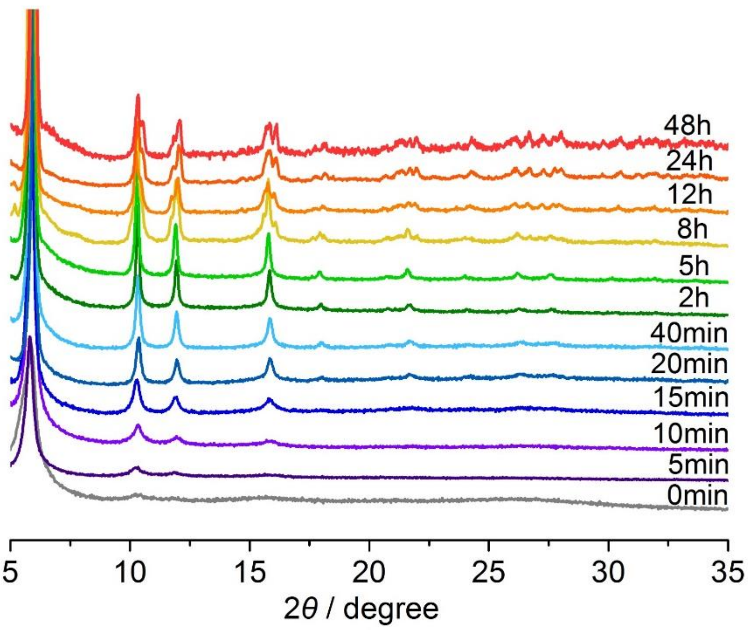

Figure S22. PXRD patterns of the products after hydrothermal reactions of $Tb(OAc)_3$ and *S*-cyampH$_2$ at pH 4.5 and 100 °C for different period of time.

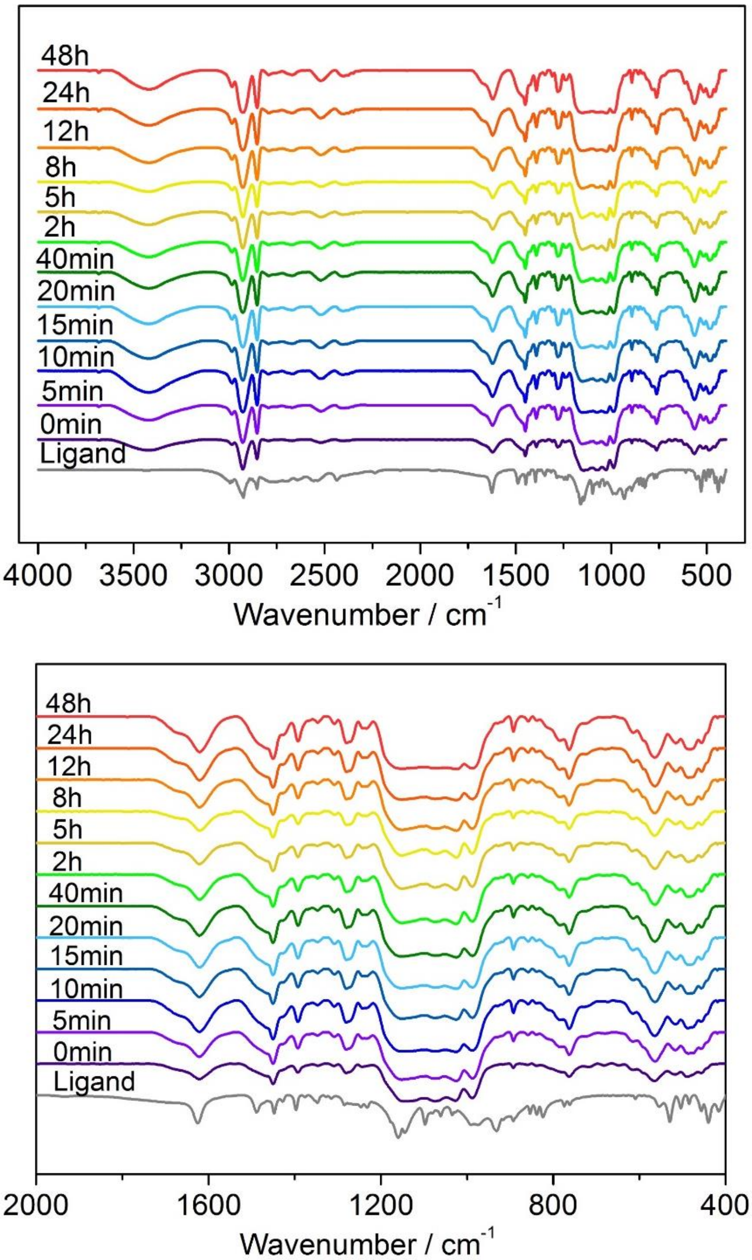

Figure S23. Infrared spectra of the products after hydrothermal reactions of $Tb(OAc)_3$ and *S*-cyampH_2 at pH 4.5 and 100 °C for different period of time.

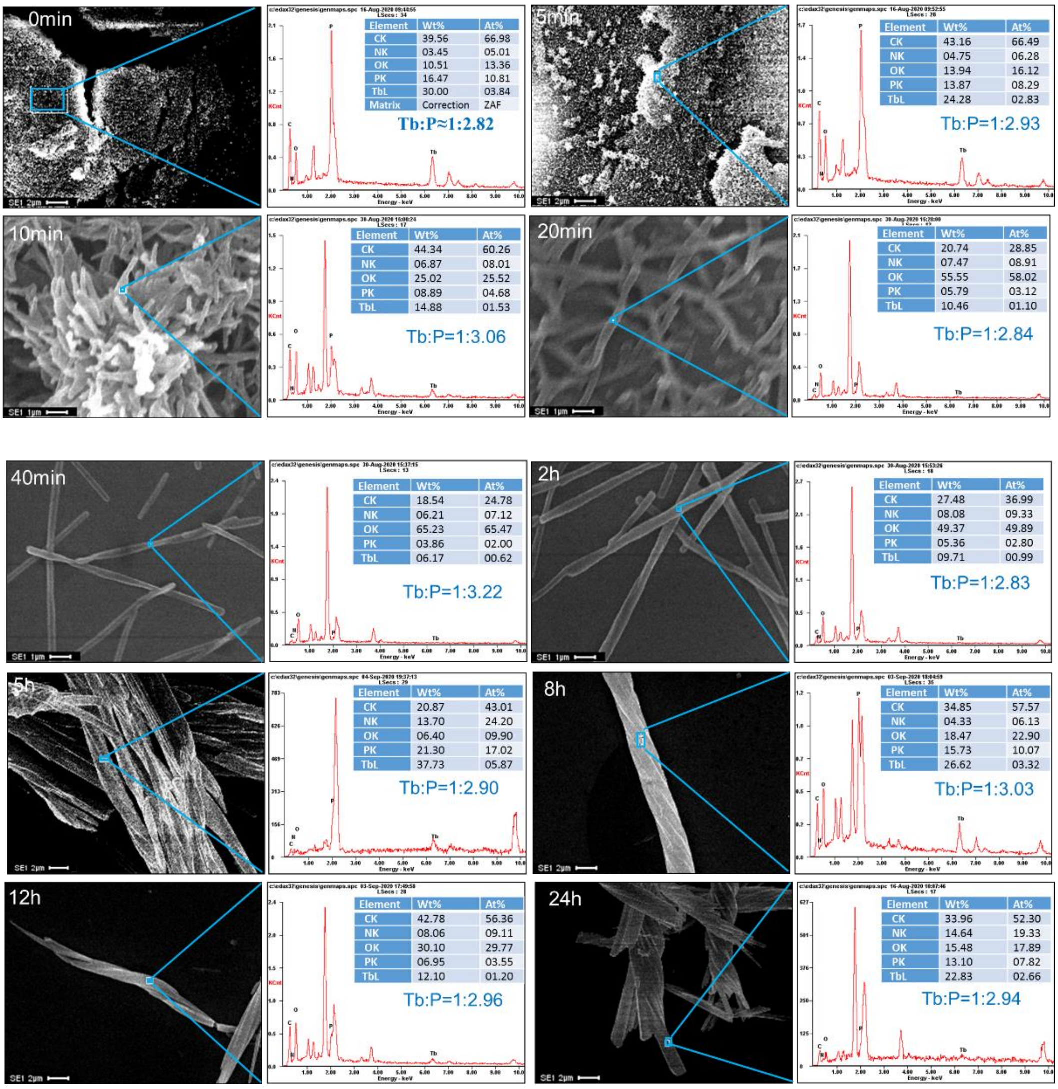

Figure S24. EDX spectra of the products after hydrothermal reactions of $Tb(OAc)_3$ and *S*-cyampH_2 at pH 4.5 and 100 °C for different period of time.

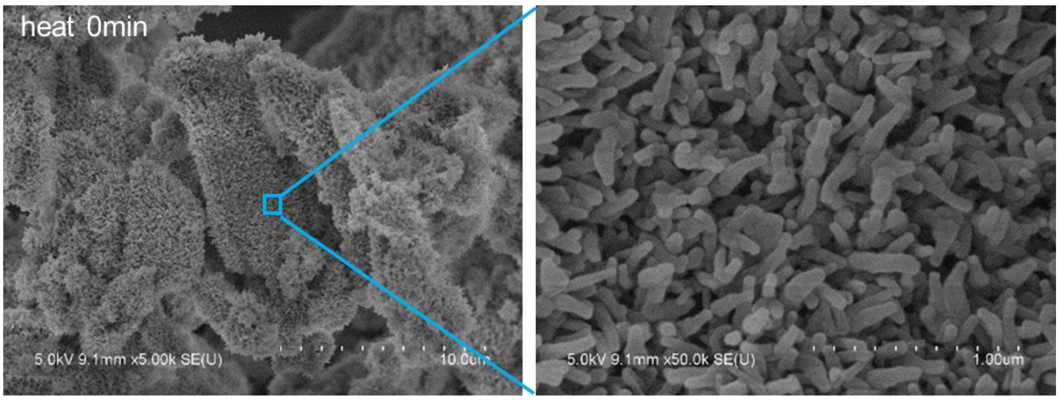

Figure S25. SEM images of the products after mixing aqueous solutions of $Tb(OAc)_3$ and *S*-cyampH_2 at pH 4.5.

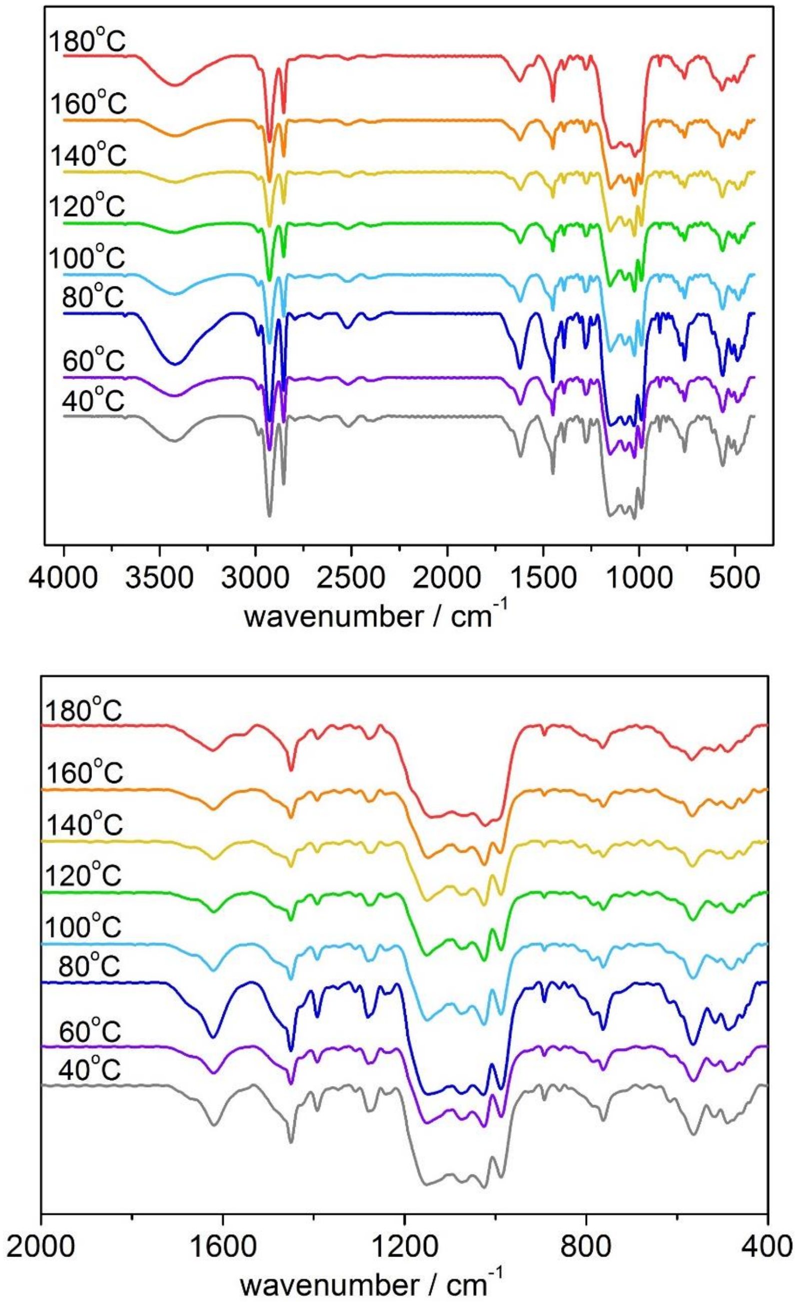

Figure S26. Infrared spectra of the products after hydrothermal reactions of $Tb(OAc)_3$ and *S*-cyampH_2 at pH 4.5 and different reaction temperature (40-180 °C) for 24 h.

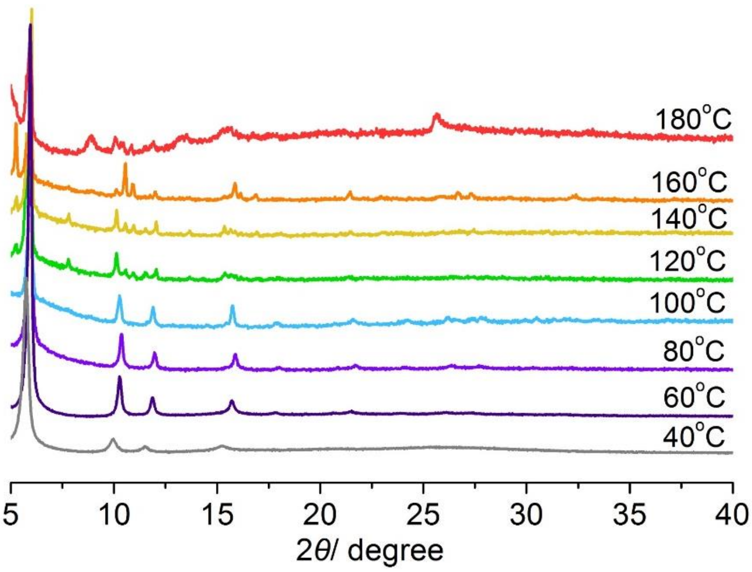

Figure S27. PXRD patterns of the products after hydrothermal reactions of $Tb(OAc)_3$ and *S*-cyampH_2 at pH 4.5 and different reaction temperature (40-180 °C) for 24 h.

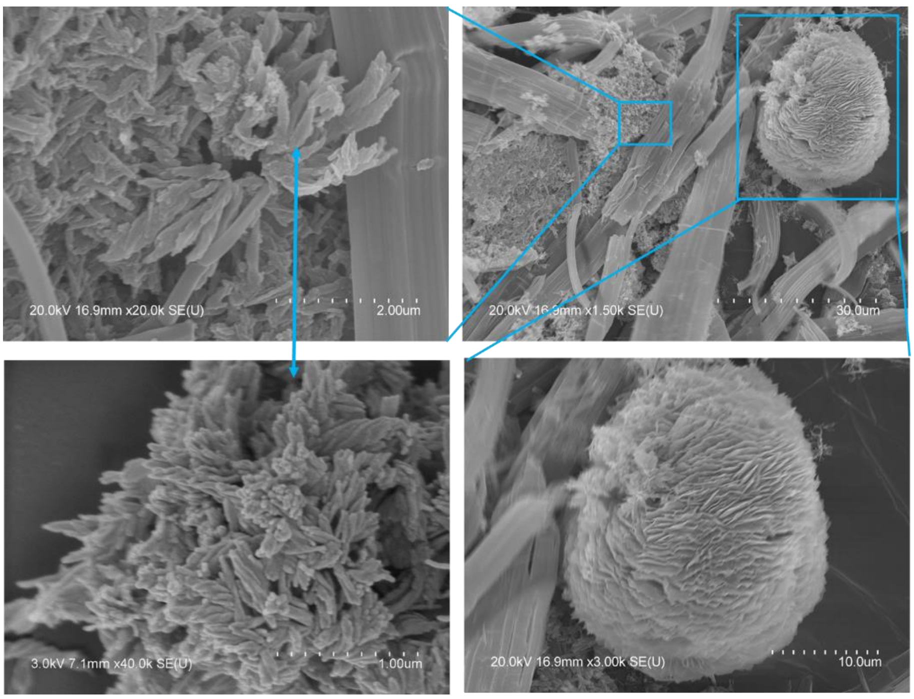

Figure S28. SEM images of the product after hydrothermal reaction of $Tb(OAc)_3$ and *S*-cyampH_2 at pH 4.5 and 160 °C for 24 h.

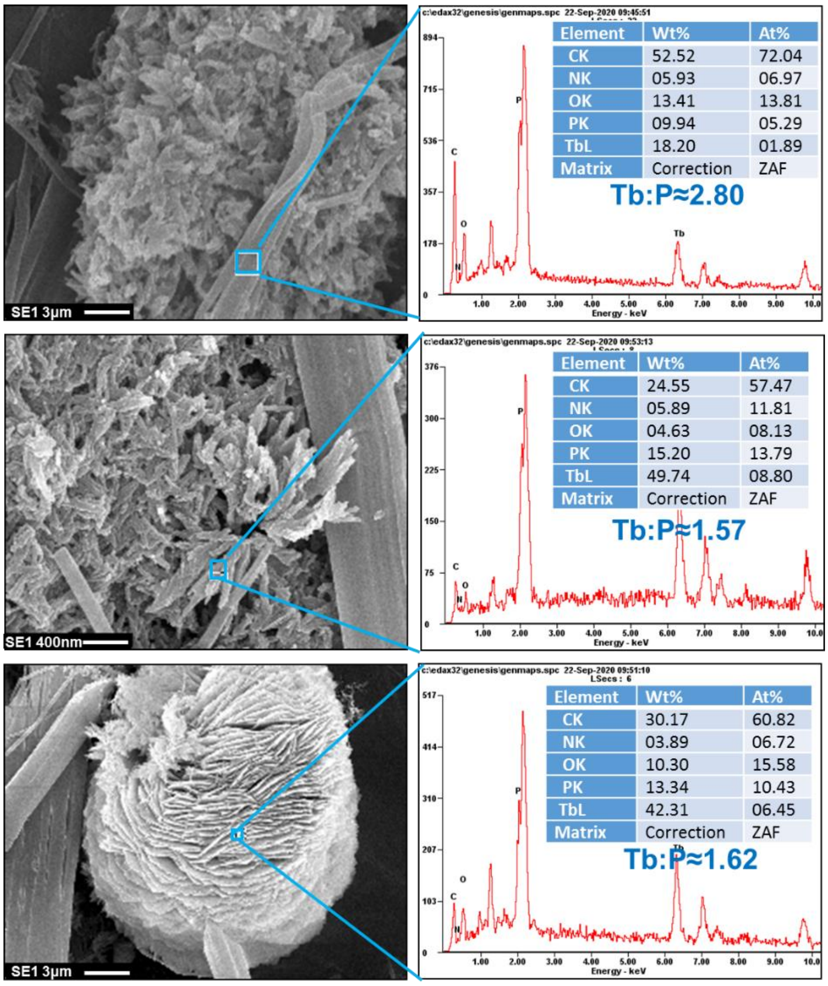

Figure S29. The EDX spectra of the product after hydrothermal reaction of $Tb(OAc)_3$ and *S*-cyampH_2 at pH 4.5 and 160 ^{o}C for 24 h.

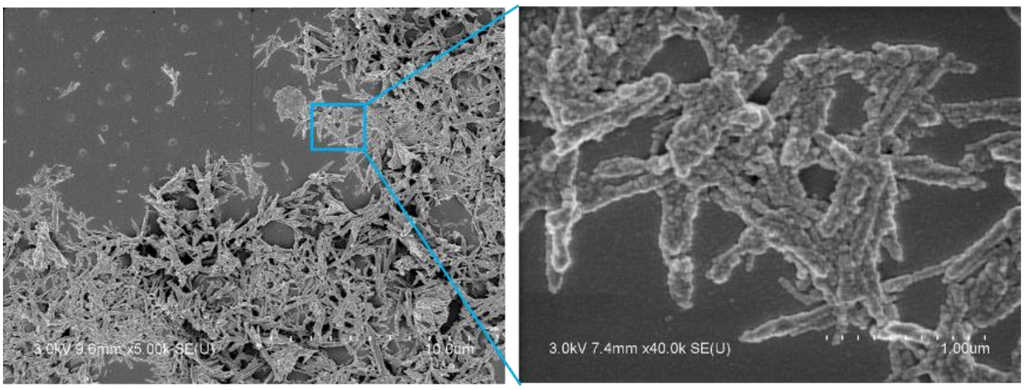

Figure S30. SEM images of the product after hydrothermal reaction of $Tb(OAc)_3$ and *S*-cyampH_2 at pH 4.5 and 180 °C for 24 h.

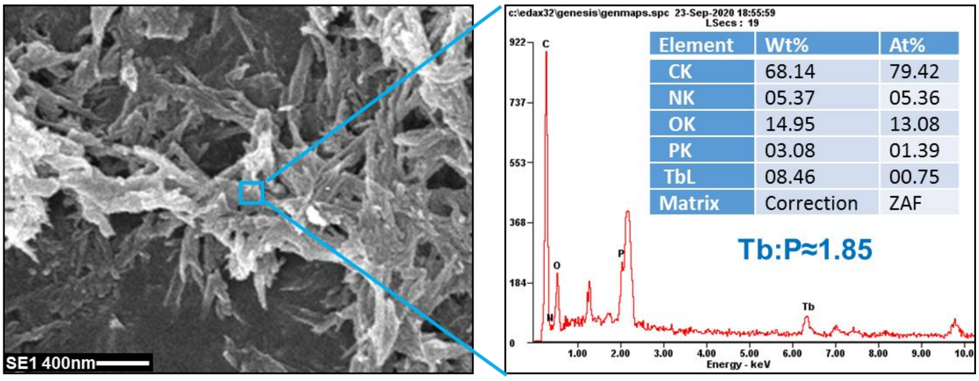

Figure S31. The EDX spectra of the product after hydrothermal reaction of $Tb(OAc)_3$ and *S*-cyampH_2 at pH 4.5 and 180 °C for 24 h.

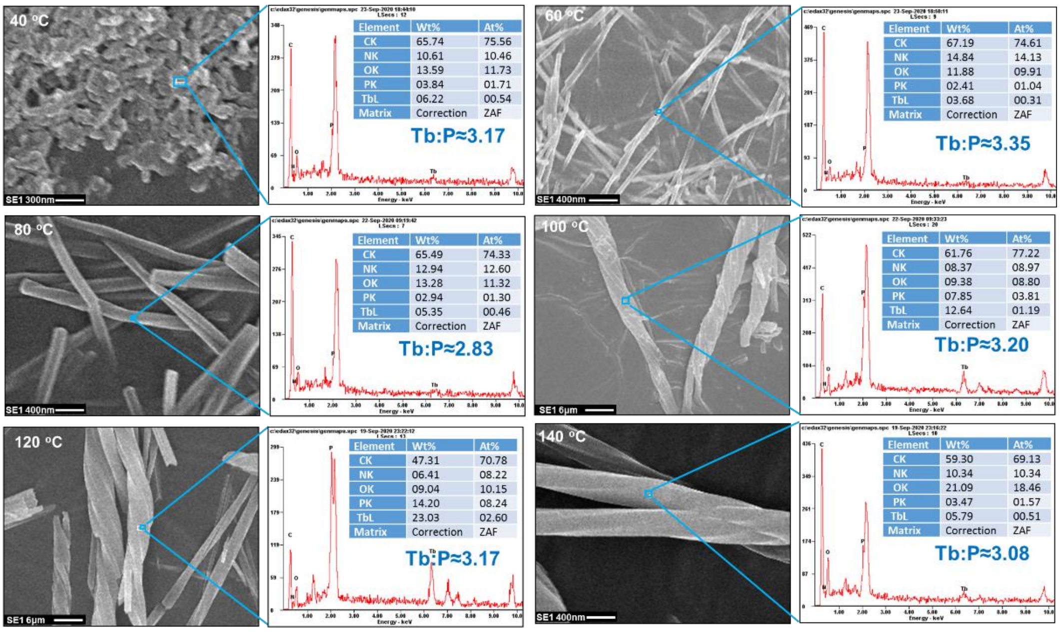

Figure S32. The EDX spectra of the product after hydrothermal reaction of $Tb(OAc)_3$ and *S*-cyampH_2 at pH 4.5 and different reaction temperature (40-140 °C) for 24 h.

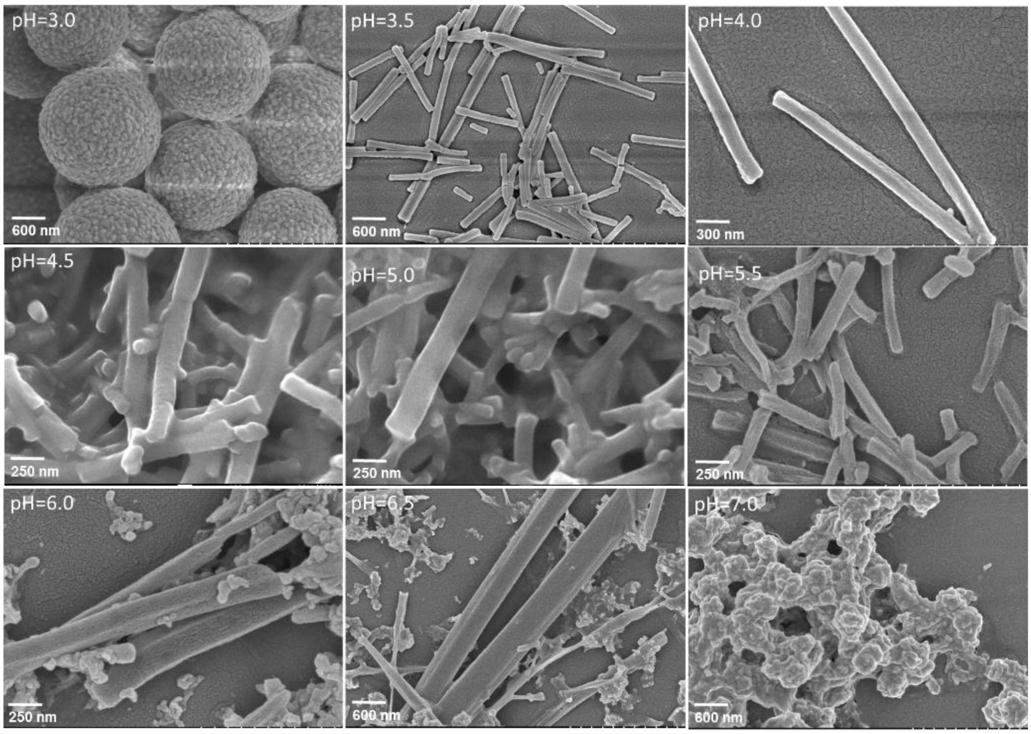

Figure S33. SEM images of reaction products using $Tb(OAc)_3$ and racemic *R/S*-cyampH_2 ligands as precursor at 100 °C for 24 h (pH = 3.0-7.0).

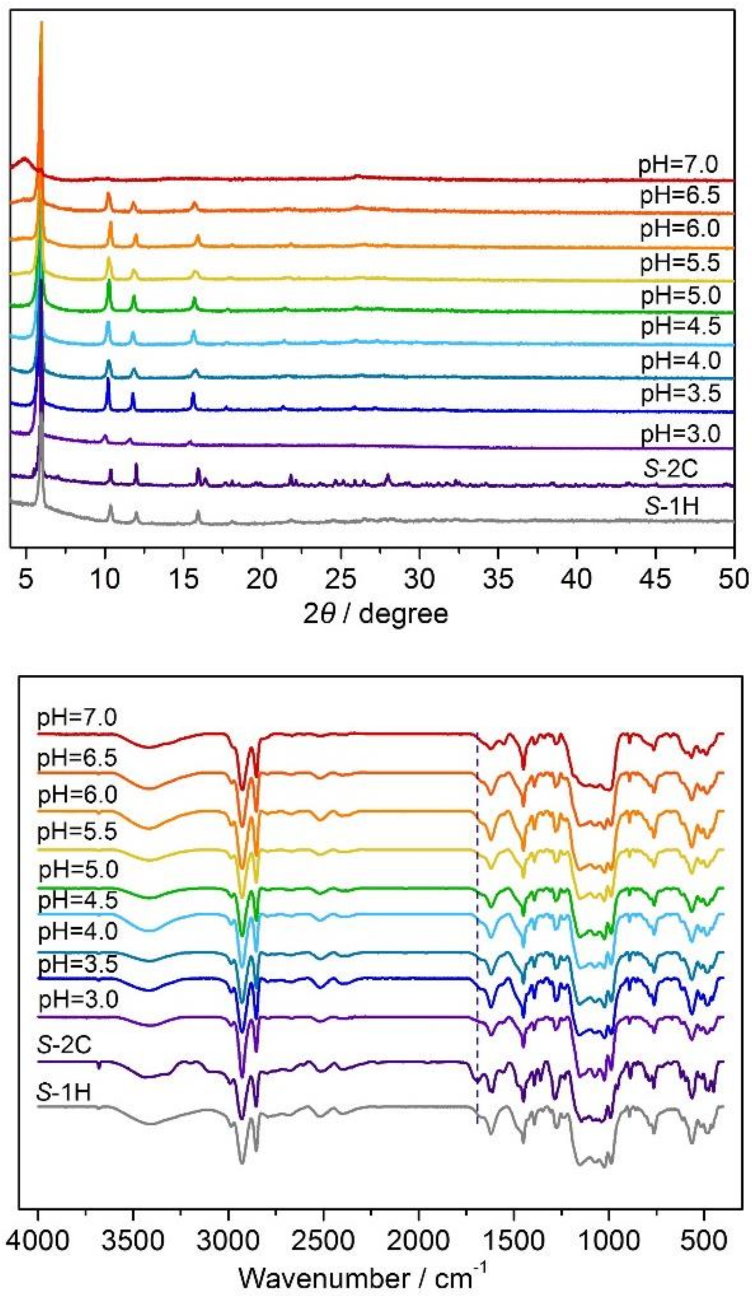

Figure S34. The PXRD patterns (top) and IR spectra (bottom) of reaction products using $Tb(OAc)_3$ and racemic *R/S*-cyampH_2 ligands as precursors at 100 ^{o}C for 24 h (pH = 3.0-7.0).

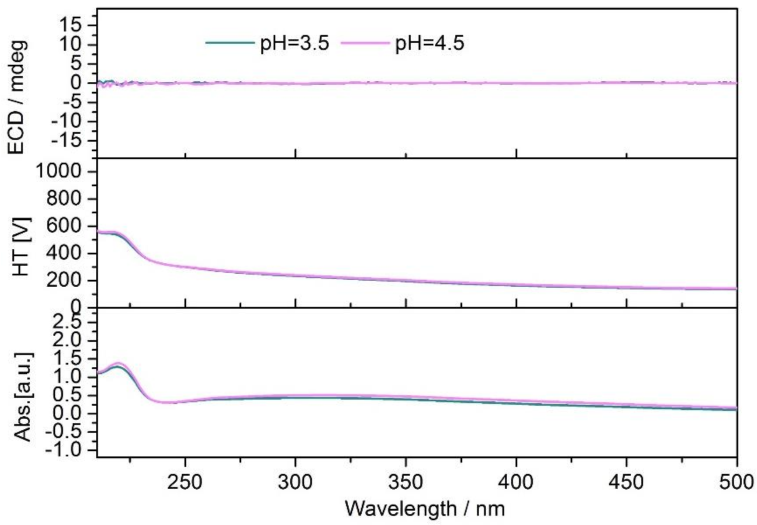

Figure S35. ECD spectra of reaction products using Tb(OAc)$_3$ and racemic *R/S*-cyampH$_2$ ligands as precursors at 100 ^oC for 24 h (pH = 3.5, 4.5).

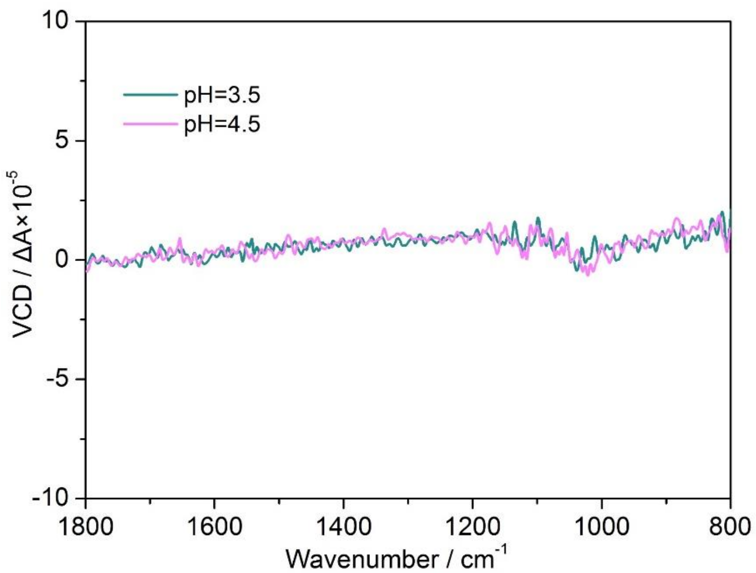

Figure S36. The VCD spectra of reaction products using Tb(OAc)$_3$ and racemic *R/S*-cyampH$_2$ ligands as precursors at 100 ^oC for 24 h (pH = 3.5, 4.5).

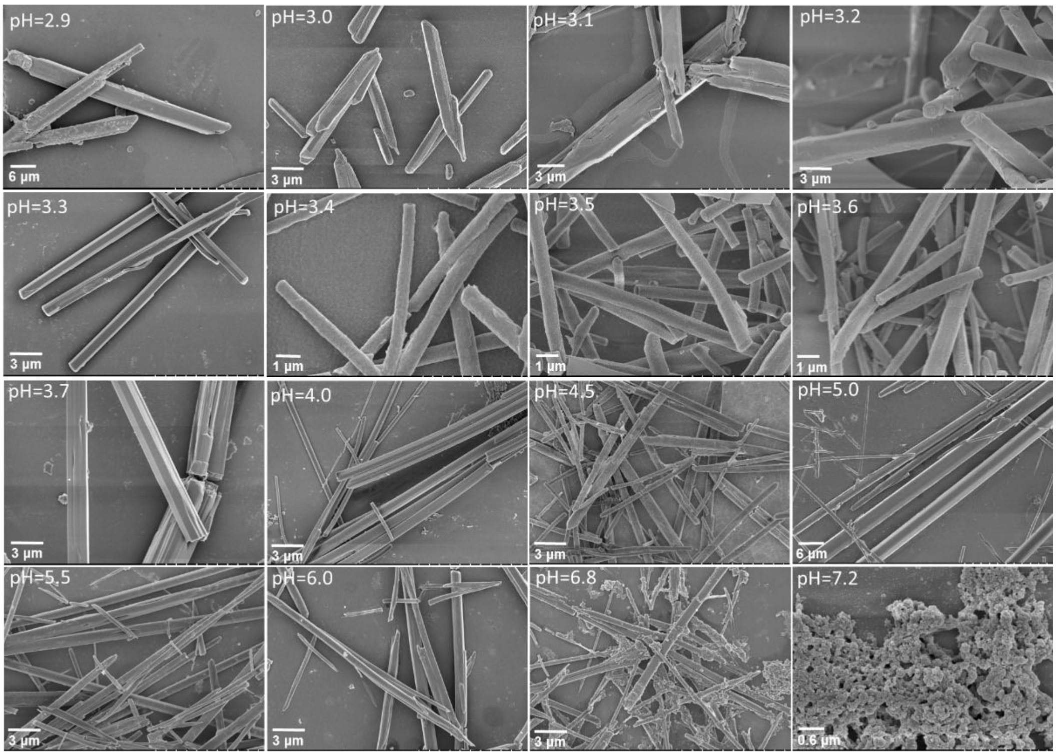

Figure S37. The SEM images of reaction products using $Tb(OAc)_3$ and *S*-pempH_2 ligand as precursors at 100 °C for 24 h (pH = 2.9-7.2).

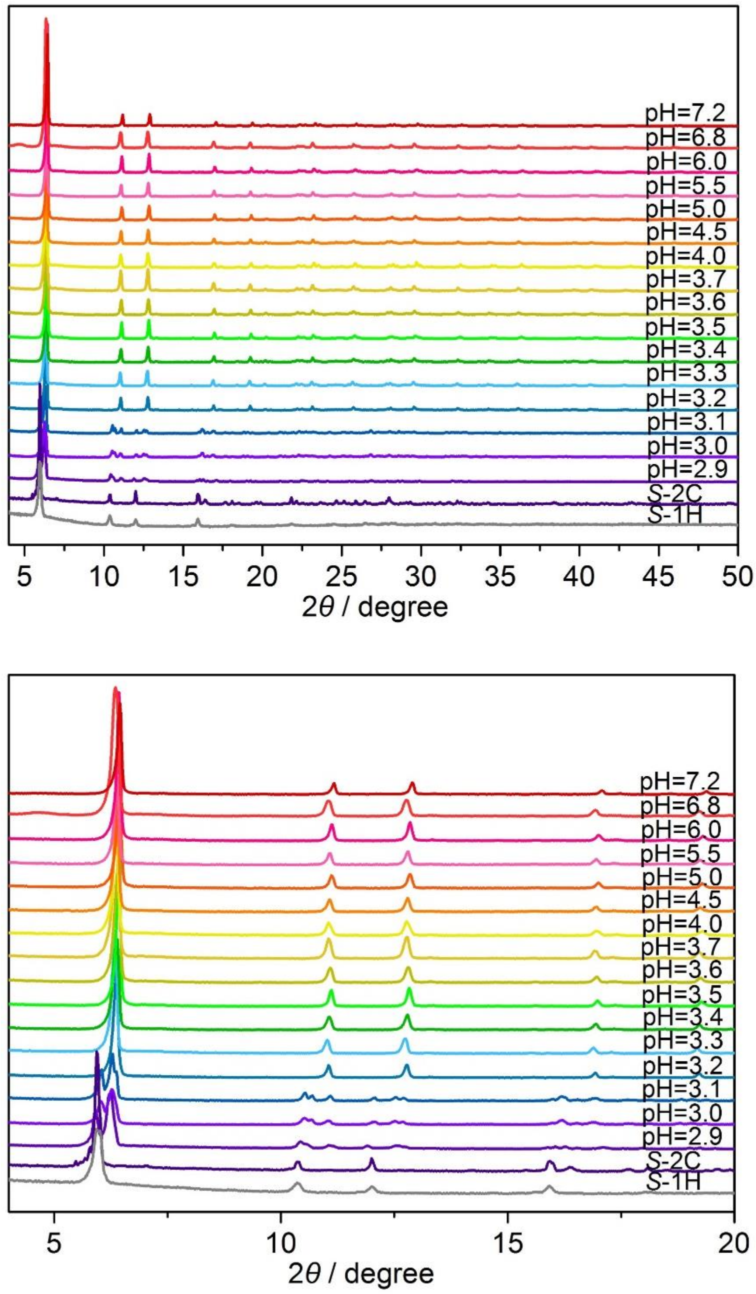

Figure S38. The PXRD patterns of reaction products using $Tb(OAc)_3$ and *S*-$pempH_2$ ligand as precursors at 100 ^oC for 24 h (pH = 2.9-7.2).

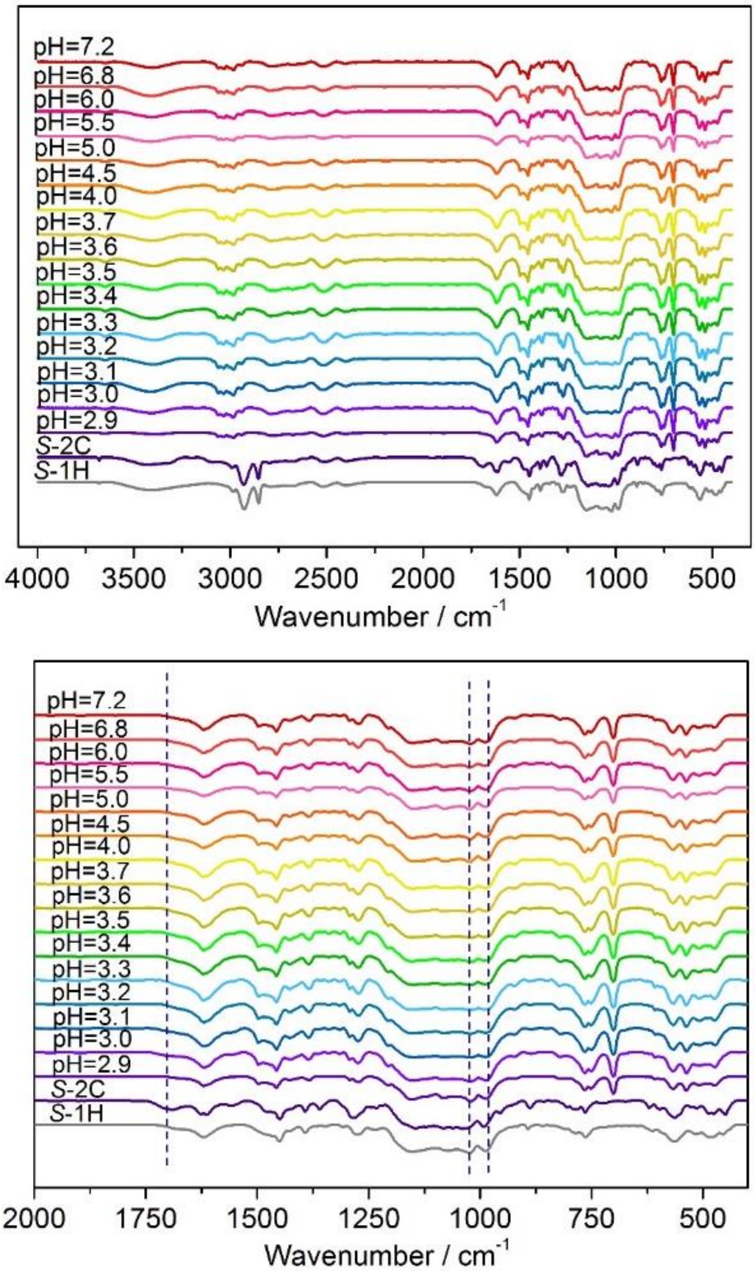

Figure S39. The IR spectra of reaction products using $Tb(OAc)_3$ and *S*-$pempH_2$ ligand as precursors at 100 °C for 24 h (pH = 2.9-7.2).

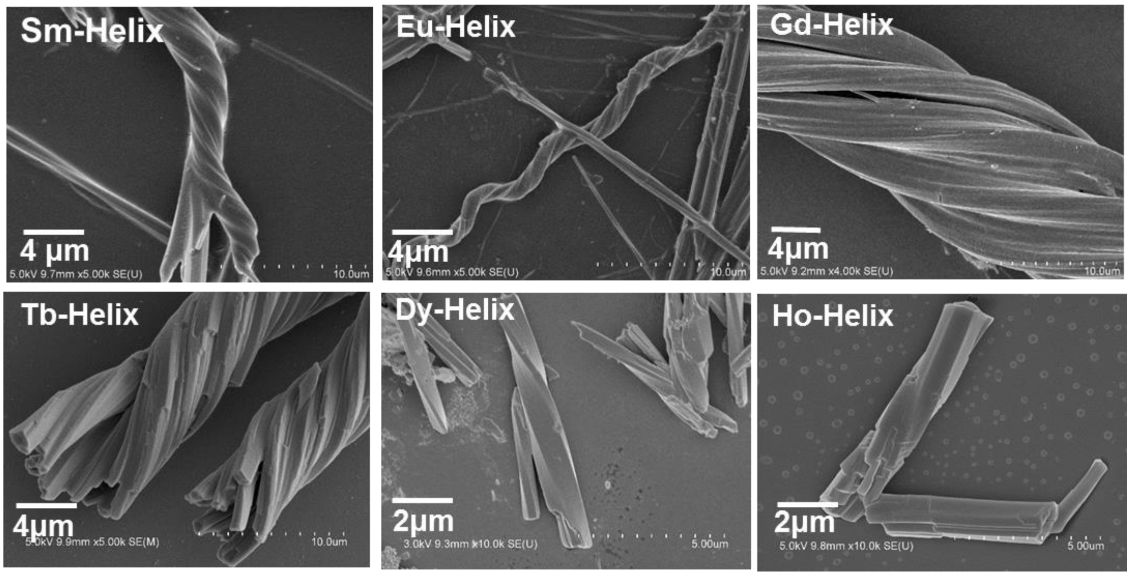

Figure S40. SEM images of superhelices obtained using different kinds of rare-earth acetate salt as reaction precursor.

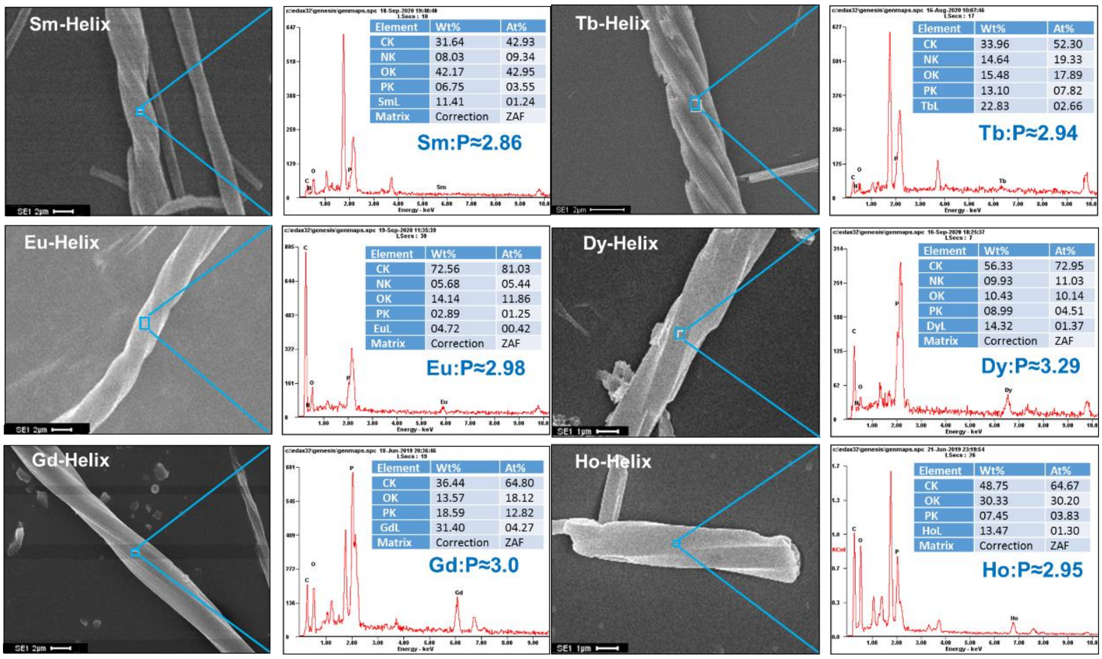

Figure S41. SEM images and EDX spectra of superhelices obtained using different kinds of rare-earth acetate as reaction precursor.

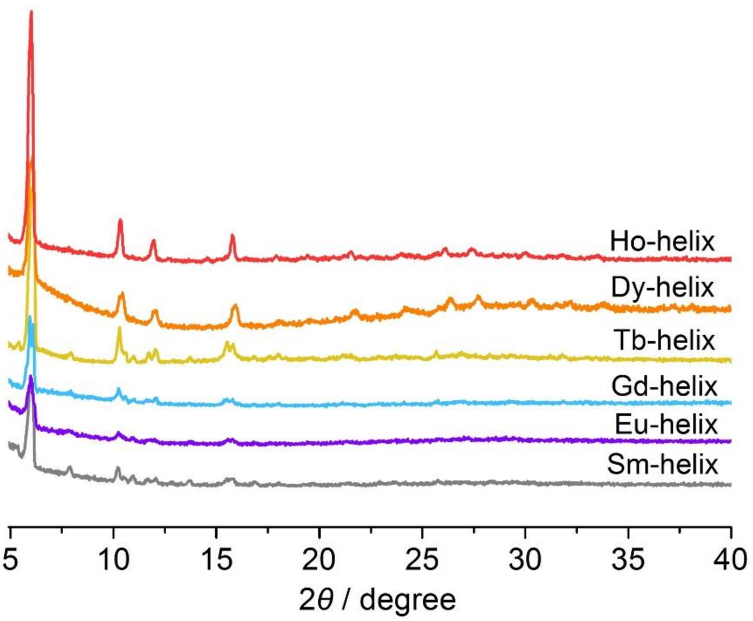

Figure S42. PXRD patterns of helices obtained using different kinds of rare-earth acetate as reaction precursor.

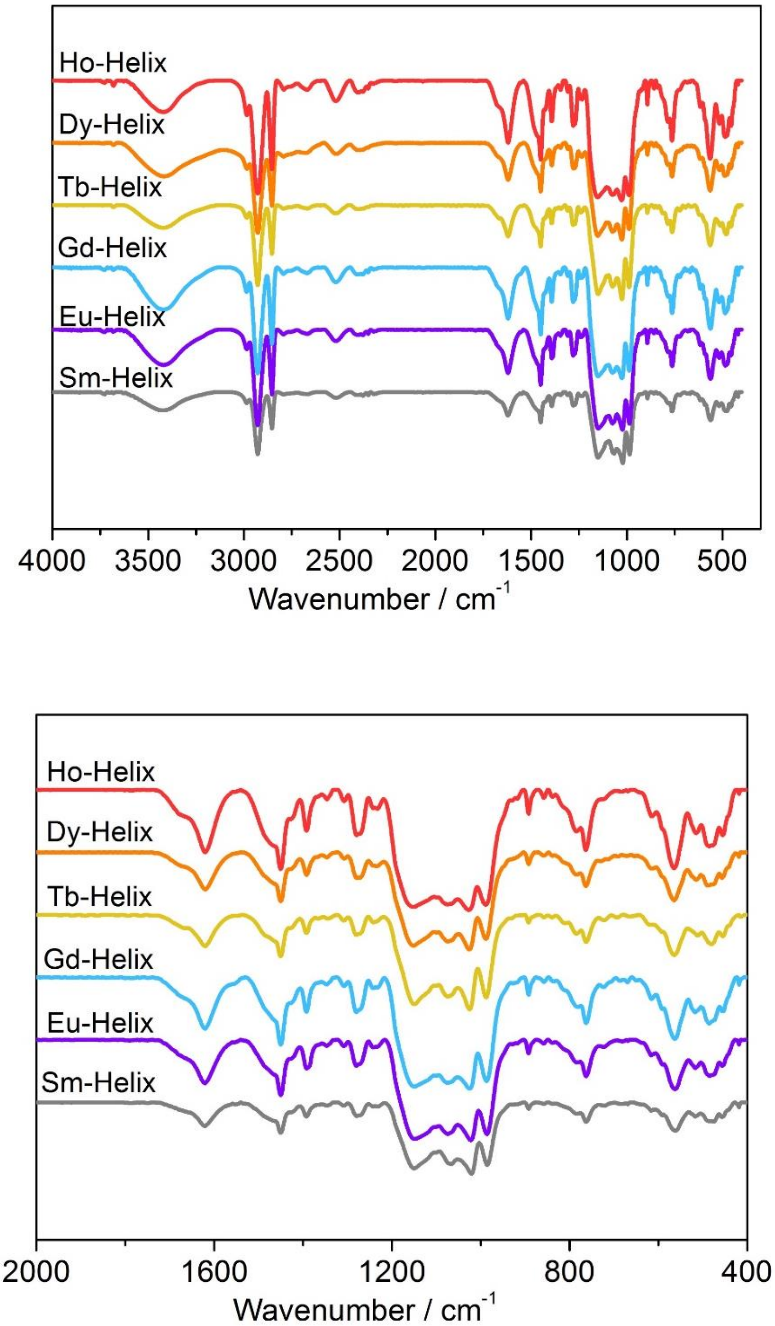

Figure S43. Infrared spectra of helices obtained using different kinds of rare-earth acetate as reaction precursor.

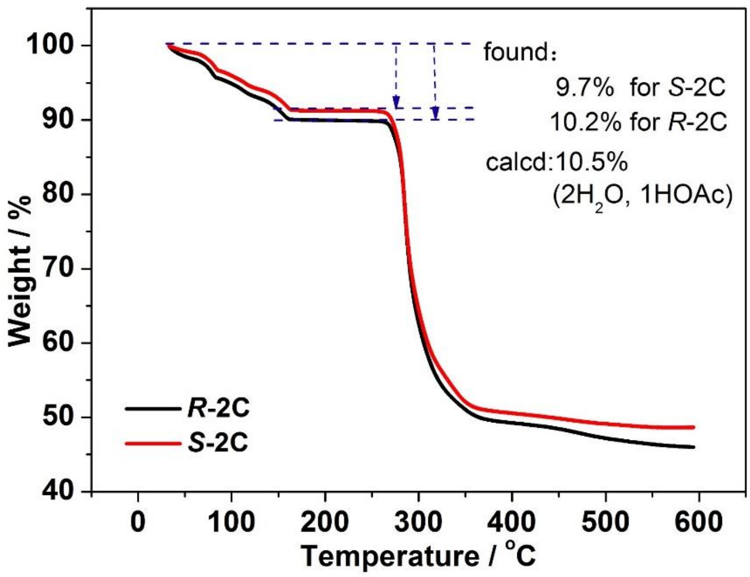

Figure S44. TG analyses of ***S*-2C** and ***R*-2C**.